Journal of Applied Physics

Particle tracking of nanoparticles in soft matter

Cite as: J. Appl. Phys. **127**, 191101 (2020); https://doi.org/10.1063/5.0003322
Submitted: 31 January 2020 • Accepted: 20 April 2020 • Published Online: 21 May 2020

Katie A. Rose, Mehdi Molaei, Michael J. Boyle, et al.

Journal of Applied Physics TUTORIAL scitation.org/journal/jap

Particle tracking of nanoparticles in soft matter

Cite as: J. Appl. Phys. **127**, 191101 (2020); doi: 10.1063/5.0003322
Submitted: 31 January 2020 · Accepted: 20 April 2020 ·
Published Online: 21 May 2020

Katie A. Rose,[1] Mehdi Molaei,[1] Michael J. Boyle,[2] Daeyeon Lee,[1,a)] John C. Crocker,[1,a)] and Russell J. Composto[1,2,3,a)]

AFFILIATIONS

[1]Department of Chemical and Biomolecular Engineering, University of Pennsylvania, Philadelphia, Pennsylvania 19104, USA
[2]Department of Materials Science and Engineering, University of Pennsylvania, Philadelphia, Pennsylvania 19104, USA
[3]Department of Biomolecular Engineering, University of Pennsylvania, Philadelphia, Pennsylvania 19104, USA

Note: This paper is part of the Special Topic on Polymer-Grafted Nanoparticles.

[a)]**Authors to whom correspondence should be addressed:** daeyeon@seas.upenn.edu; jcrocker@seas.upenn.edu; and composto@seas.upenn.edu

ABSTRACT

Recent advances in optical microscopy instrumentation and processing techniques have led to imaging that both breaks the diffraction barrier and enables sub-pixel resolution. This enhanced resolution has expanded the capabilities of particle tracking to nanoscale processes in soft matter including biomolecular, colloidal, and polymeric materials. This tutorial provides a basic understanding of particle tracking instrumentation, the fundamentals of tracking analysis, and potential sources of error and bias inherent in analyzing particle tracking. Finally, we provide a brief outlook for the future of particle tracking through the lens of machine learning.

I. INTRODUCTION

Recent developments in soft matter systems composed of mesoscopic structures with a wide range of characteristic length scales and increasing complexity present major challenges in understanding the mechanical and transport properties of these materials. The evolution of optical microscopy techniques with a resolution below the diffraction limit has allowed researchers to examine these increasingly small length scales with faster dynamics, allowing for the direct visualization of sub-micrometer processes and architectures. Particle tracking (PT, also known as multiple particle tracking) has emerged as a powerful method to characterize the dynamics in soft matter systems.

The appeal of particle tracking experiments lies in its inherent simplicity and accessibility; elegant experiments observing colloidal particles can be accomplished with just an optical microscope and a modest frame rate camera. Information about the dynamics of the probe can be extracted from the videos, which provides insight into the mechanism of probe diffusion, or the nanostructure of the biological or synthetic matrix through which the probe is transporting. While particle tracking has a rich history in using micrometer-sized colloidal probes in microrheology,[1–3] the ability to localize individual nanoscale probes, such as nanoparticles and individual fluorescent molecules, has increased the capability of particle tracking methods to investigate heterogeneous structures in soft matter systems and complex fluids. Understanding the diffusion of nanoparticles in soft matter is of both fundamental and practical interest. For example, tracking individual nanoparticles has provided new insight into understanding network heterogeneity in hydrogels,[4–6] intracellular dynamics,[7–9] transport and drug delivery within tumors,[10–13] the effect of surface chemistry on particle diffusion through mucus,[14–17] and the efficiency of nanoscale filtration methods.[18]

Tracking of larger colloidal particles has been previously reviewed in detail.[19,20] However, the underlying mechanisms governing nanoparticle diffusion and the techniques used to quantify and analyze nanoparticle diffusion pose unique challenges that make particle tracking of nanoparticles more difficult. With a focus on nanoparticle probes, this tutorial aims to address those challenges by detailing the current knowledge of nanoparticle diffusion in soft matter, as well as particle tracking methods for quantifying probe diffusion. Data extraction techniques from single and ensemble particle trajectories are described, including parameters to quantify heterogeneity, and potential sources of error in particle tracking are explained. This tutorial serves as an introduction for researchers interested in learning the basics of single nanoparticle tracking.

II. GOVERNING PHYSICS OF PARTICLE TRACKING

To understand the utility of particle tracking techniques, the underlying physics governing particle motion, particularly at the nanoscale, must be understood. The simplest case of particle diffusion, a spherical particle in a Newtonian fluid, can be modeled by the Stokes–Einstein relationship,[21] where probes are randomly diffusing by thermal fluctuations with a diffusion coefficient of

$$D = \frac{k_B T}{6\pi\eta r_h}, \tag{1}$$

where k_B and T, η, r_h are Boltzmann's constant, the temperature, the solvent viscosity, and the particle hydrodynamic radius, respectively. In Sec. V A, we will discuss more thoroughly how the mean squared displacement (MSD) can be related to time-dependent diffusivity, but for a probe diffusing in a simple viscous liquid, the MSD is related to the diffusion coefficient through

$$MSD = 2nD\tau, \tag{2}$$

where n is the dimensionality of diffusion process. In many cases, however, diffusion of probes follow a power-law scaling as $MSD = 2A\tau^{\alpha}$, where α is the power law exponent depending on particle motion and A is a constant prefactor. When $\alpha = 1$, the MSD scales linearly with time and the probe exhibits normal diffusion, as predicted by Stokes–Einstein and observed in colloidal probes moving through a fluid via Brownian motion and $A = nD$. For cases where $\alpha \neq 1$, the probe dynamics deviate from Stokes–Einstein and exhibit anomalous diffusion: for $\alpha < 1$, the probe is subdiffusive, and when $\alpha > 1$, the probe is superdiffusive.

A key assumption of Stokes–Einstein relation is that the probe particle is substantially larger than the characteristic length scale of the medium being probed. This condition is easily met for a colloidal sphere diffusing in a small molecular fluid,[22] but nanoparticle dynamics have been shown to substantially deviate from Stokes–Einstein, where the size of the probe is comparable to the characteristic length scale of the medium.[23,24] Examples of systems where the probe is in a similar length scale to its environment, where Stokes–Einstein no longer holds, are not uncommon. In polymers, when the size of a nanoparticle probe approaches the characteristic length scale in an entangled polymer melt, i.e., the tube diameter (d_t), the Stokes–Einstein model fails to adequately describe the probe's enhanced motion relative to Stokes–Einstein predictions.[25,26,26–32]

Enhanced nanoparticle diffusion compared to Stokes–Einstein predictions has been explored both experimentally and theoretically. Brochard-Wyart and de Gennes argue that as the size of a nanoparticle approaches the correlation length of a system there is a sharp crossover in the local friction felt by a nanoparticle due to the particle "feeling" the local viscosity of the monomers rather than the viscosity of the bulk, leading to accelerated particle diffusion.[33] This breakdown in Stokes–Einstein has been reported for a variety of polymer solutions[34–39] and melts.[26,29,40,41] Recent theoretical studies have also predicted deviations from Stokes–Einstein behavior, predicting a transition from bulk nanoparticle diffusivity to that associated with the local monomer or solution viscosity.[32,42] Experimentally, the Stokes–Einstein relation has been observed to hold for for $2r_h > 5d_t$, while theoretical studies indicate that this behavior occurs when the nanoparticle diameter is seven to ten times larger than d_t.[26]

Furthermore, in polymeric and biological networks with a mesh size, ζ, in the regime where $2r_h > \zeta$, subdiffusive motion is experimentally observed.[4,5,43,44] In entangled melts, Brochard-Wyart and de Gennes predict that for $2r_h > d_t$, the nanoparticle has to wait for the constraining chains to fully relax before the nanoparticle can move, producing subdiffusive behavior.[33] There are additional theories that have been derived that explain enhanced nanoparticle diffusion in these systems, including a constraint-release mechanism[32] and nanoparticle hopping.[45] Verifying theories for the mechanism of nanoparticle diffusion remains a challenge because events such as constraint-release and nanoparticle hopping are rare, require visualizing individual particles, and occur at the nanoscale, making the visualization of the individual probe dynamics and identifying these events a prominent challenge in soft matter.

While these theories account for some of the key features of nanoparticle diffusion in polymeric systems, including nanoparticle size and characteristic length scales of the system, many more factors affect nanoparticle diffusion such as grafting characteristics of the nanoparticle and particle–polymer interactions.[46,47] For grafted nanoparticles, diffusivity is expected to decrease relative to their bare counterparts, as assumptions such as no-slip at the surface of bare nanoparticles no longer hold.[33] In polymer melts, bound polymer layers have been shown to form around nanoparticles in attractive polymer–nanoparticle systems, creating long-range interactions between nanoparticles.[46] Furthermore, many industrially relevant systems for drug delivery including hydrogels,[5,48–51] cellular components,[9,52–54] and biofilms[55–58] are notoriously heterogeneous and the confinement or characteristic length scales that a particle experiences are spatially dependent. Examining how nanoparticle probes move through soft matter systems not only expands upon the current theories surrounding nanoparticle diffusion, but will allow for further development of our understanding of how these other factors contribute to nanoparticle motion.

III. PARTICLE TRACKING METHODS

There are a variety of techniques used to characterize probe mobility in soft matter that span length scales from nanometers to micrometers. Broadly, they can be characterized by (1) if the methods measure single particles or the ensemble average of particle motion and (2) by how the probe is detected, either by fluorescence or non-fluorescence. The techniques presented below are summarized in Table I, with select citations to highlight their use in particle tracking.

A. Ensemble dynamic techniques

Ensemble dynamic fluorescence techniques such as fluorescence recovery after photobleaching (FRAP),[146] fluorescence correlation spectroscopy (FCS),[147–149] and image correlation spectroscopy (ICS)[86] all utilize temporal changes in fluorescence intensity to quantify and characterize probe mobility. The spatiotemporal resolution of all fluorescence techniques is governed by the signal of the fluorescence probe; at short time scales (high temporal resolution),

TABLE I. A compilation of commonly used particle tracking techniques, sorted by ensemble or single particle tracking techniques, with references to select applications.

Sampling	Method	Select applications in particle tracking
Ensemble dynamic techniques	Fluorescence recovery after photobleaching (FRAP)[a]	Mobility in cellular membranes[59–62]
		Intracellular transport[63–67]
		Molecular interactions and conformational changes[68–71]
		Particle diffusion in biofilms[72,73]
	Fluorescence correlation spectroscopy (FCS)[a]	Mobility in cellular membranes[74–78]
		Intracellular transport[76,78–80]
		Molecular interactions and conformation changes[81–84]
	Image correlation spectroscopy (ICS)[a]	Mobility in cellular membranes[85]
		Protein aggregation[86,87]
		Molecular interactions[88]
	Dynamic light scattering (DLS)[b]	Particle size and distribution in liquids[89–91]
		Particle aggregation and gelation[92–97]
		Aging in glasses and colloidal gels[98–100]
	X-ray photon correlation spectroscopy (XPCS)[b]	Nanoparticle dynamics in polymer and micelle solutions[39,101–105]
		Nanoparticle dynamics in polymer melts[26,29,40,106]
		Aging in colloidal and nanoparticle glass[107–110]
	Differential dynamic microscopy (DDM)[b]	Bacterial mobility[111–113]
		Nanoparticle and colloidal diffusion in solution[114–116]
		Kinetics of colloidal aggregation and gelation[117,118]
	Rutherford backscattering spectrometry (RBS)[b]	Nanoparticle dynamics in polymer melts[41,46,47,119]
Particle tracking techniques	Total internal reflection microscopy (TIRF)[a]	Characterization of network structures[4–6,120,121]
		Mobility in cellular membranes[122–125]
		Intracellular dynamics[7–9]
		Particle–surface interactions and adsorption dynamics[126–129]
	Dark field microscopy (DFM)[b]	Cell mechanics[130–134]
		Gels and polymer solution[135,136]
		Membranes and interfaces[137–140]
	Interferometric scattering microscopy (iSCAT)[b]	Label free tracking of viruses and proteins[137,141,142]
		Molecular motor dynamics[143]
		Mobility in cellular membranes[144,145]

[a]Fluorescence based techniques.
[b]Non-fluorescence based techniques.

few photons are emitted from the fluorescent probe resulting in poor spatial resolution. Conversely, at long time scales, the increase in fluorescence intensity results in an increase in spatial resolution, but temporal resolution decreases accordingly. Due to a high fluorescent signal from the bulk diffusion of multiple probes, these techniques have excellent signal even with short exposure times, resulting in a temporal resolution in the microseconds.[68] This comes at the loss of information about distinct particle populations to ensemble averaging, as individual probes cannot be distinguished.

For ensemble dynamic scattering techniques, including dynamic light scattering (DLS),[150] x-ray photon correlation spectroscopy (XPCS),[151] differential dynamic microscopy (DDM),[152] and Rutherford backscattering spectrometry (RBS),[153] high temporal resolution is achievable (ns to ms) but spatial resolution is dictated by the detectable q-range and the size of the probe. For DLS and DDM, the q-range is limited by the use of a coherent light source while XPCS can access substantially smaller length scales due to its use of coherent x-rays from a synchrotron source. The temporal resolution of scattering techniques are generally improved over that of fluorescence measurements, as fluorescence measurements are limited by fluorescence saturation, i.e., where no photons are emitted, for extremely small time scales.[154] Furthermore, depth profiling methods, such as RBS, measure the concentration profile which can be fit with a diffusion equation to determine the coefficient. A wide range of probe sizes can be used in these techniques, from nanometers to several micrometers, as the limitation comes from the resolution of the instrument and technique, rather than the probe size.

RBS differs from the previously mentioned bulk scattering techniques in that it is an *ex situ* measurement, where the measurement

is on a "glassy" sample. Thus, the shortest annealing time is determined by the limitations of the annealing chamber to drive diffusion. While the spatial resolution is typically 70–100 nm, the *ex situ* nature of the technique means the accessible time scales are much longer than the previously mentioned techniques, on the order of minutes to days.[153]

Although the above approaches yield valuable information on the dynamics of processes at the nanoscale, they have substantial limitations for understanding particle motion. While useful for examining the ensemble average diffusion, these techniques cannot identify distinct mechanisms of the diffusion of different populations since single particles cannot be spatially resolved. Relevant systems including polymer melts, complex fluids, and biological systems have local heterogeneity on the nanoscale and characterization techniques need to be able to distinguish different populations of probe mobility to extract useful nanoscale structural information. It is in these cases that particle tracking methods can be powerful in extracting spatiotemporal characteristics of a diffusing probe.

B. Particle tracking techniques

Particle tracking (PT) encompasses a series of techniques that track individual particles in 2D or 3D. The bulk of this tutorial will focus on 2D translational particle tracking, though many of the ideas outlined here have analogous or similar counterparts in 3D and rotational tracking. Rotational and 3D tracking microscopy techniques will be described briefly. Broadly, particle tracking methods can be divided into two categories based on the method of observation and visualization: (1) fluorescence based particle tracking and (2) non-fluorescence based particle tracking. For both of these sub-classes, the overall method is similar: a video camera records images of a sample at specific time intervals, capturing particle positions at different time points. Image series are then processed to identify particles, record their positions, and determine particle tracks by linking particle positions between frames. The general schematic is detailed in Fig. 1, and some of the most common fluorescence and non-fluorescence techniques for colloidal and nanoparticle tracking are outlined below.

1. Fluorescence based particle tracking techniques

Particle tracking experiments have been largely dominated by fluorescence based microscopy, as the emergence of fluorescent labels catalyzed the improvement fluorescence optical methods to visualize biological structures. In epifluorescence mode, all incident light from the laser source is passed through the sample, illuminating probes both in the imaging plane and in the background. The collected light is, therefore, a combination of the emission from probes in the image plane, all probes in the foreground and background, and the excitation light that has been reflected off the glass interface. Dichroic mirrors, which reflect select wavelengths of light while transmitting others, and other optical filters are used to separate the excitation light from the sample emission. Epiflourescence typically has a low signal-to-noise ratio due to the contribution of out of focus probes to the background signal, which can limit the tracking of small molecules and probes.[155] Illumination techniques that limit the background noise, such as total internal reflection fluorescence (TIRF) microscopy, are used to increase the contrast between single probes and the background by only exciting probes in the specimen plane. TIRF microscopy utilizes the phenomena of total internal reflection to produce an evanescent wave in the medium that illuminates a narrow region of the sample near the interface, approximately 200 nm from the cover glass. This eliminates any contribution from fluorophores above the imaging plane, producing images with a high signal-to-noise ratio.[156] An example of a TIRF microscopy set up is detailed in Fig. 2.

Variations of TIRF microscopy have further enhanced the range and scope of particle tracking. In particular, multi-color channel implementations have been heavily utilized in biological applications to image molecular interactions.[157–160] In this setup, either a single multiline laser or a laser combiner is used to deliver multiple laser beams with different wavelengths to the sample. To visualize the probe emissions at different wavelengths, either multiple cameras via a multi camera adaptor is utilized or a beam splitter is used to project the multiple emissions onto different sections of a single detector.[161] Furthermore, the principles of TIRF have been combined with other fluorescent imaging techniques including photoactivated localization microscopy for single particle tracking (SPT-PALM).[162] In SPT-PALM, photoactivated chimera proteins are switched between their active forms, which allows for their position to be recorded, before photobleaching to return the proteins to their "off" state. Subsequent iterations of activation, localization, and photobleaching small subsets of the diffusing populations allows for individual proteins to be resolved and SPT-PALM has been used to image protein dynamics in crowded and heterogeneous spaces such as membranes.[162,163]

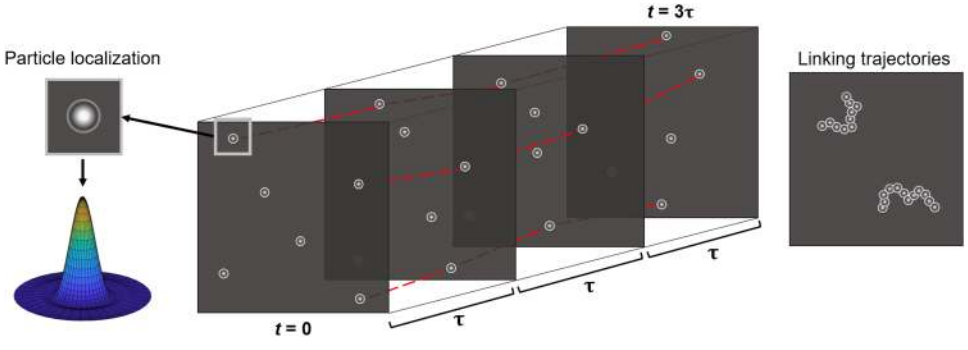

FIG. 1. A schematic of the process of particle tracking from particle localization to linking trajectories. In a single frame, individual particles are localized (far left) and positions identified by fitting the point spread distribution function, an Airy disk, using algorithms outlined in Sec. IV D. Between subsequent frames determined by the lag time, τ, trajectories are linked (red dashed lines), creating trajectories for individual particles (far right).

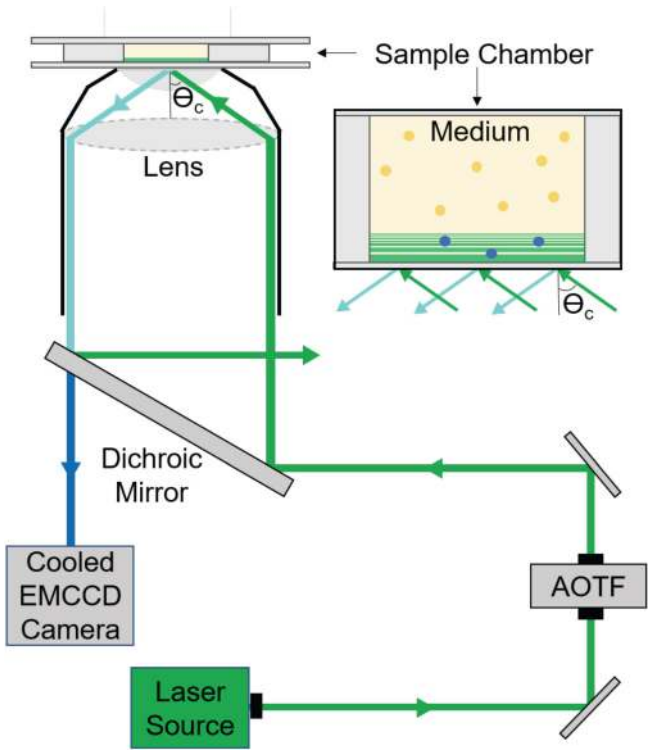

FIG. 2. A schematic of a TIRF microscopy setup. A laser is guided to the objective through a series of lenses and passed through an acousto-optic tunable filter (AOTF) to regulate irradiation intensity. While light passes through the cover glass at a high incident angle, at a specific critical angle, Θ_c, the light is completely reflected producing a ~200 nm evanescent wave into the sample. Probes in the region of the evanescent wave are excited and the reflected emission is passed through a dichroic mirror to allow light from the probe emission to pass through to the EMCCD and deflect any reflected light from the laser source. The sample chamber is composed of two cover slips spaced between two glass slides, and then sealed to prevent evaporation.

2. Non-fluorescence based particle tracking techniques

Although much of the literature, particularly nanoscale tracking, has been focused on fluorescence methods, non-fluorescence based techniques such as dark field microscopy have been increasingly utilized as they are not limited by some of the difficulties faced by fluorescence measurements; some examples of these difficulties include photobleaching of proteins and molecules, photoblinking of QDs, and the required labeling of biomolecules or probe of interest with fluorescent molecules.

Dark field microscopy (DFM) has been introduced as an alternative to simple bright field microscopy to enhance the signal to noise ratio and resolution of imaging of label-free particles. In DFM, the light scattered from the sample is collected while unscattered illumination light is blocked and not collected by the detector. The corresponding images of particles formed in DFM are bright spots in a dark background. Based on this common concept, many different configurations have been developed for DFM imaging. The conventional DFM configuration is similar to bright field microscopy with a special illumination light, in which the center portion of the light is blocked and only a ring of light is focused by the condenser at the specimen plane, see Fig. 3(a). The oblique angle in DFM should be larger than the numerical aperture, otherwise they will be collected by the objective. One inefficient way to block the central light and generate oblique light source is to use spider stops in front of the condenser, since it blocks the major portion of the light. The alternative method is the use of an axicon lens to generate a ring light [Fig. 3(b)].[164–166] As shown in Fig. 3(c), epi-illumination through an objective can also be used for dark field imaging. In this method, however, the back-scattered light from the particles is captured by the imaging system that often has a smaller electrical field compared to forward scattered light.[167–169] An alternative method to epi-illumination is using planar illumination which is normal to imaging axis, Fig. 3(d).[170] Because contrast is based on scattering, signal strength scales with illumination intensity. This allows high frame rate (kHz–MHz) imaging of nanoparticles[171] without the photophysical limitations (bleaching, blinking, and limited photon emission rates) detrimental to fluorescent techniques.[171–174] As a scattering based technique, signal strength in DFM depends on the ratio of light scattered from particles of interest to spurious background scattering events (which prove difficult to eliminate). Since the scattering cross section for the particles with

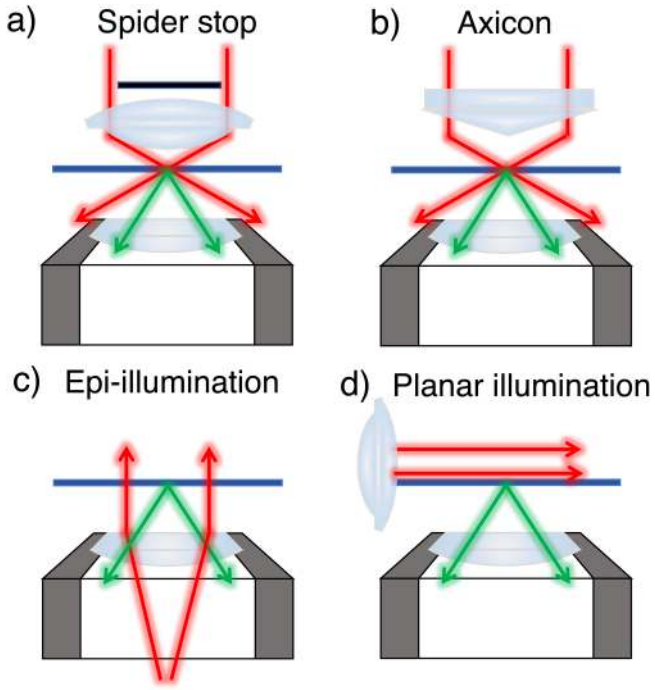

FIG. 3. Optical path of different configurations of dark field microscopy using (a) spider stop in front of the condenser, (b) axicon lens, (c) epi-illumination, and (d) planar illumination. Red lines are illumination beams and green lines are image forming beams.

diameter, a, smaller than the wavelength of light scales with a^6, noble particles such as gold and silver have become popular choices as tracers in DFM due to their strong optical signals in the visible and near IR range. The unique optical properties of noble metal nanoparticles arise from their localized surface plasmon resonance, which will be further discussed in Sec. IV B 1.

Rather than relying on pure scattering to generate signal, interferometric scattering microscopy (iSCAT) techniques operate by imaging the interference between light scattered by a probe with a reference beam, i.e., reflected light at the glass/sample interface. The constructive and destructive interference of the light scattered with the reflected beam serves as the contrast mechanism[173] and particles appear as a dark spot in a larger bright background signal. Compared to DFM, the signal from particles in iSCAT scales with a^3 as opposed to a^6, which enable this technique to image much smaller nanoparticles. The total noise in iSCAT is dominated by the reflected beam, negating the impact of spurious background scattering events that dominate DFM, and enhancing interferometric contrast.[171] This background suppression allows for label free imaging of weakly scattering materials (proteins, viruses)[174] and smaller particles (~5 nm).[172] It is important to note that because any particle or object with a refractive index different than the surrounding medium will scatter light, scattering based techniques lack the specificity of fluorescence based techniques which isolate imaging to a particular fluorescent object.[171]

3. Rotational particle tracking

It has recently been shown that nanorods, in comparison to chemically identical spheres, exhibit increased and anomalous diffusion in mucus,[175] the interstitial matrix of tumors,[176] polyacrylamide spheroids,[177] and wormlike micelles[104,178–180] highlighting growing interest in anisotropic particle diffusion. For an anisotropic probe, there is both lateral and axial diffusion perpendicular and parallel to the rod axis, as well a rotational diffusion component.[181] While conventional optical microscopy, such as confocal microscopy,[182–184] can view the effective rotational diffusion of large anisotropic particles, more complex approaches must be taken to identify the rotational component of nanoprobes since their physical sizes are smaller than the diffraction limited resolution of optical microscopy.

To track the rotational motion at the nanoscale, nanoprobes with anisotropic optical proprieties are used. For example, the intensity gradient in the microscopic image formed by a fluorescent sphere-doublet can be used to deduce its angular orientation. In this technique, the eigenvectors of the moments of the intensity distribution reveal the symmetry lines.[185,186] However, the most common way to determine the orientation of the nanoprobes is based on the emission characteristics of the electric dipoles. In these methods, aberrated[187,188] or defocused[189,190] images of the dipoles are recorded, and information obtained from the formed patterns is used to measure the angular orientation.[191–193]

Besides fluorescent nanobeads, recently, gold nanorods have been utilized as ideal orientation probes. Local surface plasmon resonance of a gold nanorod strongly depends on its orientation with respect to external electric fields. Many optical microscopic imaging[130,131,139,194–199] and depolarized scattering techniques[200–202] have been introduced to track the rotational motion of gold nanorods. For example, we have developed a nanoscale rheology technique based on tracking the rotational motion of gold nanorods in complex environments. We use laser-illuminated dark-field microscopy and optical polarization to determine three-dimensional orientation of gold nanorods.[198]

4. 3D particle tracking

Fast diffusion of nanoparticles in materials with low viscosity makes imaging with 2D microscopy systems difficult due to the rapid axial motion of particles out of the field of view, demanding 3D imaging techniques. Beyond confocal scanning microscopy, several optical microscopy techniques have been developed that are suitable to track fast 3D motion of nanoparticles. One example is digital holographic microscopy (DHM), which has been extensively employed to track 3D motion of micrometer size colloids,[203–206] and has recently been utilized for nanoparticle imaging.

In a basic DHM setup, a sample is illuminated with a coherent light source; the interference pattern of this coherent light (reference beam) and scattered light from the colloids (object beam) form the holograms which contains the 3D content of the image information.[207] There are two complementary methods to analyzing digital holograms. In a method based on Fourier diffraction theory, three-dimensional light field is reconstructed to generate a 3D image. This 3D image is then used to identify position, shape, and the orientation of colloids.[204,208,209] In the second method, images are fit to predictions of the Lorenz–Mie theory to determine the position of the colloids, their size and shapes, and even their index of refraction.[205,210] In general, particles with a larger index refraction compared to that of surrounding are more suitable for holographic microscopy. Since biological colloids often have a small index refraction, incorporating dyes have been shown to improve both amplitude and phase contrast.[211] Although recording magnified holograms through implementing DHM in comparison to lens-less holography[212] enable this technique to track submicrometer particles, 3D imaging of nanoparticles requires further alteration to the conventional DHM.

While in conventional DHM where coherent light sources are used as an illumination as well as a reference light source, incoherent digital holography[213] has been introduced to track the 3D location of fluorescent nanoparticles.[214,215] Furthermore, by combining dark field microscopy and DHM, Verpillat *et al.*[216] were able to track the 3D motion of 100 nm gold nanoparticles in water. Because of the weak intensity of the scattered light from nanoparticles, their imaging requires an illumination light source with intensity beyond the saturation limit of sensor chips of normal cameras. Utilizing dark field operation in DHM alleviates the saturation issue of the sensors by blocking the illumination beam.

Heterodyne DHM has also been successfully implemented for 3D localization of gold nanoparticles.[217] In heterodyne DHM, the reference beam is dynamically phase shifted[218] or frequency shifted[219] with respect to the signal field. Using this technique, a strong reference beam can be mixed with a very weak signal, making it suitable for photon level detection. The heterodyne DHM with total internal reflection configuration of dark field microscopy has enabled the 3D detection of 50 nm gold nanoparticles in thick

samples (up to ∼ 50 μm deep).[217] Furthermore, photothermal excitation can be used to detect metallic nanoparticles with DHM to increase precision.[220] In this method, one laser is used to heat the particles and create a local refractive index change, while another laser is used as the local oscillator beam to create holograms. The sensitivity of this method and the absorption efficiency of the metallic nanoparticles enable tracking nanoparticles down to a nanoparticle diameter of 10 nm.[220]

IV. PRINCIPLES OF PARTICLE TRACKING

As mentioned previously, the basics of particle tracking are quite simple: the movement of a particle is captured using video microscopy, and recorded images are subsequently processed and analyzed to yield the locations of the probe and its trajectory (Fig. 1). The most technically challenging part of particle tracking is creating a system that yields clean images with easily identifiable particles. In this section, we outline instrumentation requirements that create optimized images for particle tracking, provide options for fluorescent and non-fluorescent probes, and detail how to process images to yield useful and accurate data regarding nanoprobe mobility.

A. Microscopy requirements

1. Camera and detector

There are a variety of detector options when choosing a high performance scientific camera, primarily a charge-coupled device (CCD), electron-multiplied CCD (EMCCD), intensified CCD (ICCD), and scientific complementary-metal-oxide-semiconductor (sCMOS) detectors. All CCDs contain silicon diode photosensors that release an electron into a storage region when photons with a sufficient energy hit the detector. An amplifier then reads out the accumulated charge collected over the exposure time, which is converted to voltages and subsequently converted to digital values. CCDs and EMCCDs are limited to modest frame rates, approximately 70 frames per second (fps) for a 512 × 512 pixel array due to the process of the stored charge moving through registers sequentially prior to analog to digital conversion.[221] EMCCDs have a similar structure to regular CCDs, but the stored charge is passed through a multiplication register which further amplifies the charge, increasing the signal to above that of the read-out noise even at high read-out speeds.[222] Both CCDs and EMCCDs are susceptible to high thermal noise, and may necessitate additional cooling components for proper tracking in low-light experiments.[223] ICCDs utilize an image intensifier in front of a CCD to amplify incoming light, increasing the signal read by the detector. While ICCDs are also susceptible to thermal noise from the image intensifier, the amplified light is often above the thermal noise of the CCD detector; therefore, additional cooling components are not needed. Additionally, ICCDs contain a shutter functionality; the passing of electrons to the CCD is controlled by a small pulsed gate voltage, which allows for ICCDs to have much faster shutter speeds than a conventional CDD, on the order of picoseconds.[224] While the frame rate of ICCDs is limited to that of the EMCCD or CCD, the repeated acquisition of a signal through gating can produce a larger signal than that acquired through a CCD alone. Last, sCMOS detectors have an amplifier attached to each pixel in the sensor with each column of pixels connected to an analog to digital converter. This results in increased frame rates, up to 1000 fps for a 512 × 512 pixel array, and lower read-out noise compared to EMCCDs and CCDs. However, as every pixel has its own individual amplifier, each pixel has a unique noise associated with it, which can make image denoising, discussed later in tracking algorithms, difficult.[221,225]

Overall, the choice of a camera is highly dependent on the types of experiments to be performed. For example, in low-light applications with modestly bright probes the use of a cooled EMCCD would be appropriate, as the cooled system would reduce thermal noise (see Sec. IV C 2) and the EMCCD would increase the signal of the probes. Conversely, in the case of tracking sufficiently bright colloidal particles a CCD could be appropriate, and the use of intensifiers and coolers most likely is not necessary.

2. Objective lenses

The choice of objective lens not only determines the magnification of the sample but also the image resolution. In a diffraction limited system, probes do not appear as a single bright spot but rather a point spread function (PSF), a three-dimensional diffraction pattern that appears in the two-dimensional plane as a spot with concentric rings of decreasing brightness; mathematically, these rings can be described as Airy disks. The ability to distinguish two discrete particles depends on the size of their Airy disk patterns, which is directly related to the numerical aperture of the objective and the wavelength of light as described by the Rayleigh criterion,[226]

$$d_l = \frac{0.61\lambda_0}{NA} = r_A, \tag{3}$$

where d_l is the maximum lateral-resolving power, λ_0 is the wavelength of incident light, NA is the numerical aperture of the objective, and r_A is the radius of PSF described by an Airy disk. Individual particles can be resolved when the distance between them is larger than d_l, or interchangeably, r_A. High numerical aperture objectives, such as oil immersion objectives, are commonly used in nanoparticle tracking as increasing the numerical aperture decreases r_A. For example, for a illumination light with a wavelength of 532 nm, a 60× objective with a numerical aperture of 1.4 (an oil immersion objective) yields a $r_A \sim 230$ nm, whereas an air immersion objective with the same magnification but NA smaller than 1.0 increases the r_A to ∼ 325 nm, an approximately 100 nm decrease in resolution. Furthermore, as Airy disk patterns are well described mathematically, any aberrations and deviations in the patterns such as asymmetric rings are indicative of an improper microscope alignment or damaged optical components and must be resolved prior to data collection. Failure to do so will result in improper fitting during the particle localization step and a loss of precision.

The depth of field, an estimate at which a particle remains in focus, is also governed by the numerical aperture and the wavelength of light for large numerical apertures[227]

$$d_a = \frac{n_s\lambda_0}{NA^2}, \tag{4}$$

where n_s is the sample refractive index. This quantity is particularly important for systems with highly diffusive particles or for extended experiments, as particles that move out of the axial limit of resolution become more difficult to resolve and localize in most particle tracking algorithms.

3. Reducing external perturbations

When tracking at the nanoscale, small perturbations can have disastrous effects. For successful tracking, both the sample itself and the microscope should be carefully isolated. Perhaps the most obvious source of perturbations are vibrations, resulting from fume hoods and blowers for air handlers, small fans on electronics, or cooling systems, or even movement and talking from those conducting the experiments. To reduce these vibrations, the use of an isolation table is critical. Furthermore, in any room, there are air currents from the heating and cooling of the building and these can cause substantial drift if the microscope is not isolated either with a curtain or an environmental chamber.

B. Sample consideration

1. Probe selection

For particle tracking experiments to be successful, the selection of the probe must be carefully considered. First, the probes must be stable during the time scale of the experiment. A lack of probe stability arising from either the aggregation of particles or chemical degradation of the probe can limit the range of accessible timescales. In colloidal particle tracking, there is the concern of particle sedimentation, though this is less of an issue with the use of nanoparticle probes, where the time scale for sedimentation is much longer than a typical particle tracking experiment, and thermal diffusion is sufficient to overcome gravitational sedimentation. Additionally, the probe must either emit enough light or generate significant contrast in the cases of fluorescent and non-fluorescent PT, respectively. Otherwise, the exposure time of the detector must be increased to compensate the weak signal, which, in turn, can cause dynamic error as discussed in Sec. V A 2. Last, if the goal of the experiment is to probe the nanoscale structure of the material, the probes should be homogeneous in both size and shape. Probe uniformity is especially important in particle tracking, as the reported diffusion coefficient is inversely proportional to the particle size. Small changes in probe size, therefore, have a drastic impact on the slope of the MSD, and can artificially suggest system heterogeneity.

Commonly used probes for fluorescence based particle tracking are fluorescently labeled particles, proteins, and organic dyes. Fluorescent beads, such as polystyrene and silica, are advantageous due to their wide commercial availability, which offers an impressive range of absorption/emission spectra and sizes ranging from tens of nanometers to several micrometers. Fluorescent dyes can either be incorporated within the particle itself during particle synthesis or covalently attached to the surface.[228–232] In biological experiments, fluorescent proteins and dyes are advantageous due to their small size ($<$5 nm) and biological relevance. In particular, dyes are often used to tag biomolecules of interest as their small size does not sterically hinder interactions with other biomolecules or cellular components. Additionally, there is a large library of well established bio-conjugation methods that enable researchers to attach dyes to a variety of biomolecules.[233] Various fluorescent proteins and dyes are also photoswitchable or photoactivatable, a necessary property for techniques like SPT-PALM.[234] However, both proteins and fluorescent molecules are of limited use for particle tracking due to their low photostability over time; the onset of photobleaching occurs on the time scale of milliseconds for fluorescent proteins and several seconds for organic dyes, reducing the precision of tracking or eliminating the ability to track particles all together for long experiments. The above mentioned probes are also brightness limited, with their relatively low photon flux (even prior to photobleaching) limiting tracking precision.[235]

With both high photostability and high quantum yield, semiconductor quantum dots (QDs) have become increasingly prominent in imaging applications where extended experimental times limit the use of fluorescent molecules due to photobleaching, or increased fluorescence is necessary for tracking precision. QDs are highly tunable nanometer-scale semiconductor crystals, between 2 and 10 nm, with a narrow emission and broad absorption spectrum modulated by the core size,[236] composition,[237] and surface ligands;[238] this enables their use in a range of experimental set ups including multi-channel tracking systems. However, a limitation of the use of QDs as probes in particle tracking arises from the photoluminescence intermittency, or "blinking," as the particles transition between illuminated and non-illuminated states.[239] This can lead to difficulties in linking probe trajectories as particles disappear between subsequent frames.

For non-fluorescence based particle tracking, the most commonly used probes are silica, polystyrene, or gold. The advantages of non-fluorescent silica and polystyrene are similar to those of their fluorescent counterparts; there is a wide variety of sizes that are available commercially and the particles exhibit excellent scattering properties. Gold nanoparticles are especially useful in DFM due to their superior absorption and scattering of light compared to other similarly sized nanoparticles. The key to this increased scattering lies in the surface plasmon resonance effect or the collective oscillation of surface conduction electrons at a specific wavelength of light. The optical properties of gold are highly dependent on particle size, with smaller nanoparticles absorbing below 520 nm, and larger sizes showing the absorption peak broaden and shift to higher wavelengths.[240] Generally, gold nanoparticles with diameters above 40 nm are used as bioimaging tags or probes in DFM as larger nanoparticles have an increased scattering cross section, though gold nanoparticles diameters $<$ 20 nm have been used to label biomolecules in iSCAT.[241] Other plasmon resonant metal particles, such as silver, can also be used, though the wide commercial availability of gold makes it a more attractive choice for most researchers.[242]

Both non-fluorescent and fluorescent probes can be further modified through the use of small ligands, grafted polymers, or the attachment of specific targeting moieties. Small ligands and grafted particles can be used to modify the chemical functionality of the surface of the probe, mediating interactions with the surrounding medium. Additionally, the use of grafted polymers reduces the potential for aggregation of diffusing particles by adding a steric repulsion; as particles are driven to aggregate by attractive van der

Waals interactions or depletion interactions, grafted chains keep particles stable during experimental tracking.[243] The attachment of targeting moieties is of particular interest in biological tracking as it allows for the direct imaging and sequestering of probes in a region of interest. The available chemistry for functionalizing silica,[244] gold nanoparticles,[245] and polystyrene[246,247] are well established; particles can be rendered hydrophobic or hydrophillic with the addition of small ligands and polymers which are readily grafted to and from the particle surface.[248] QD functionalization chemistry is less established, though QDs have been modified to be hydrophilic by exchanging hydrophobic ligands on the QD shell with a hydrophilic ligand or adding a second shell layer composed of a hydrophilic component, such as silica.[249] The addition of a ligand or a second shell can also provide reactive groups for subsequent biological coupling, though these modifications increase the size of the probe, limiting their applicability in experiments targeting nanoscale structures.[7,250]

2. Sample chamber

A proper sample chamber should shield the sample from external stresses and environment. A schematic of a simple hand-built sample chamber is detailed in Fig. 2, where the sample is sealed between two cover slips using glass slides, additional cover glass, or two-sided tape as spacers. The exposed edges can be sealed using epoxy or nail polish for non-biological samples. Sealing the sample not only reduces external drift but also prevents fluid convection due to evaporation of the sample during the experiment, which is particularly problematic for volatile solvents. Additionally, care should be taken to allow the sample to equilibrate on the microscope stage prior to imaging, including after handling and allowing the sample to reach thermal equilibrium by heating.

The thickness of the cover glass is objective dependent, though most objectives require the thickness to be between 0.13 and 0.17 mm thick, corresponding to a No. 1 or No. 1.5 cover glass. High precision cover glass can also be used, which has a more stringent manufacturing tolerance, reducing the range of thickness from 0.16 to 0.19 mm for No. 1.5 to 0.18–0.19 mm for No. 1.5H. Additionally, cover glass slides must be vigorously cleaned prior to tracking; possible cleaning procedures of cover glass include piranha etching or a combination of solvents and UV-ozone.[251] Utilizing the proper cover glass thickness and cleaning procedures ensures that a minimum amount of intensity is lost due to optical aberrations, improving particle tracking.

While there is a vibrant sub-section of the particle tracking field that measures the contribution of hydrodynamic effects on probe dynamics near interfaces,[126,127] in most particle tracking applications, any interactions with or due to surfaces are undesirable. For experiments in which the goal is to examine the bulk behavior of probe mobility, the thickness of the spacers must be optimized in order to remove possible hydrodynamic interactions with the confining walls. In general, the thickness of sample should be approximately 200× larger than the radius of the probe, or $T_{\min} > 200 r_h$ if the imaging plane is at mid-height.[252] The same applies for the separation from the side walls, or the spacers, of the sample. As a reference, a nanoparticle with a radius of 10 nm should then be imaged at least 1 μm from any wall.[3]

C. Image quality

1. Signal-to-noise

Precision in particle tracking is almost exclusively related to the signal-to-noise ratio (SNR) of the image: maximizing SNR increases the theoretical localization precision of individual particles. The SNR of a point source on a dark background is defined as

$$SNR = \frac{\langle I_S \rangle - \langle I_N \rangle}{\sigma_N^2}, \tag{5}$$

where $\langle I_s \rangle$ is the average intensity of the particles, $\langle I_N \rangle$ is the average intensity of the background, which includes everything except the particles in the focus plane, and σ_N^2 is the standard deviation of I_N.[253] A commonly cited threshold for good particle tracking is a SNR above 5,[254] which can be difficult to achieve for biological samples, where the SNR is traditionally poorer due to the autoflourescence of cells and the change in the refractive index between the cover glass and the sample.[255] In practice, a SNR of 2 yields a localization precision of 60 nm while a SNR of 10 yields a precision of 10 nm, highlighting the importance of optimizing SNR in experiments where high tracking precision is necessary.[256]

In addition to increasing SNR by simply using a brighter probe, there are alternative methods to optimize SNR and improve probe localization precision. The background in the SNR calculation encompasses everything but the in focus particles, including the fluorescence or scattering contribution of out of focus particles. Reducing the concentration of probe particles can, therefore, increase SNR by reducing the background intensity. Additionally, decreasing the magnification can lead to an increase in SNR, as the light emitted or scattered from the probe is concentrated in fewer pixels, increasing the apparent intensity of the probe. Optimizing the SNR is a complicated process; the probe concentration must be high enough for adequate tracking statistics but low enough to decrease contributions from out of focus particles, and decreasing the objective magnification to increase probe brightness can also reduce the PSF of the probes to less than three pixels, which can introduce pixel biasing during particle localization (see Sec. V A 5).[19] As such, there is no standard set of instrument parameters that is optimized for every particle tracking experiment, but understanding the contributions to image quality and choosing the appropriate camera, objective, and probe is critical in producing clean images with high SNRs.

2. Camera noise

Regardless of how well the system has been optimized, there is system noise that decreases image quality. The most common sources of systematic noise are shot noise, dark current, and read-out noise. Inherent to all imaging systems, shot noise, otherwise known as photon noise, results from the statistical fluctuations of photons emitted from a source; for any given imaging interval, there is underlying noise due to the variation in photon arrival at the detector. As the signal, S, increases due to an increase in photons hitting the detector shot noise, n_s also increases as $n_s \sim \sqrt{S}$.[257] Dark current is due to the thermally generated electrons within the detector that mimic the signal produced by

imaging photons, even in the absence of light.[223] Finally, read-out noise is created within camera electronics as electrons are converted from analog to digital signals, and then amplified and processed to create an image.[222]

What noise dominates for an individual experiment relies on the intensity of the image signal. In practice, the use of cooled CCDs nearly eliminates the effects of dark current noise as it is related to the temperature of the detector.[223] Depending on exposure time, image quality is limited by either read-out or shot noise. In low-light conditions, arising from either a lack of photons generated by the probes or short exposure times, read-out noise will dominate. As exposure time increases and more photons are detected, the SNR increases until shot noise is much greater than dark current and read-out noise; at this point, the image quality is shot noise limited.

D. Tracking and linking tracks

This section aims to outline the steps to successfully identify, localize, and link particle trajectories. Additionally, source code and tutorials for applying these techniques are available for a variety of coding languages, including IDL,[258] MATLAB,[259] and Python.[260]

1. Pre-processing the images

Capturing high quality images is one of the key factors in particle tracking. However, as previously explained, the recorded images often contain various sources of noise and imperfection that must be removed before locating the particles. For example, out of focus images of dust on the camera or optics and debris on the sample slides introduce a steady background noise or imperfect illumination, leading to non-uniform background brightness [Fig. 4(a)]. To separate and remove the noise, I_N, from the signal, I_S, during image enhancement, we first need to understand the source of the noise to choose the proper pre-processing technique.

Steady background: In the case that the signal in the images (location of particles in this context) is unsteady and dynamic, but the background is stationary (such as scattering light from debris on the optics), the noise image can be estimated by averaging pixel intensity over a time series of recordings, $I_N(x, y) = \frac{1}{N}\sum_1^N I(x, y)$, where $I(x, y)$ is the intensity of a pixel at (x,y) location. An alternative to averaging pixel intensity to calculate the noise image is to use median pixel intensity. Additionally, background noise can also be estimated by capturing images in the absence of particles.

Dynamic background: In case that noise in the images is not steady, removing time averaged background noise will not lead to proper noise free images. For instance, in any imaging technique with a coherent light source, the speckle noise and system noise are temporally coherent. In these imaging systems, the unsteady noise of the images should be estimated for each frame. An example of this technique is the correlation-based de-noising algorithm developed for enhancing the image of particles with low scattering signals.[261]

Nonuniform background brightness and noisy pixels: Many particle tracking algorithms rely on the ratio of intensity of the particles and the surrounding background. Therefore, any low frequency background intensity variation such as Gaussian noise or high frequency sharp noises such as salt-and-pepper noise result in errors in particle tracking. Removing these noises is possible background subtraction [Fig. 4(b)] and several filtering processes such as median and bandpass filtering [Fig. 4(c)]. Many of these filtering processes are implemented within particle tracking software, but often require input parameters from the users. These input parameters include the cutoff frequency of the bandpass filter and window size of the median filter. These parameters should be selected cautiously to properly remove the noises without altering the signal.

Ideally, after image enhancement, the resulting images from fluorescent or dark field microscopy will consist of bright spots on a dark background, with each bright spot corresponding to an individual particle. In images recorded by bright field microscopy, the particles are identified by dark spots on a bright background. As most general particle tracking codes have been written to accommodate fluorescent tracking, the simplest way is to invert the image by subtracting the pixel intensity from the maximum intensity value in the image format.

2. Locating position of particles

After image enhancement, the next step is to identify the location of the particles in the images [Fig. 4(d)]. Although the resolution of the microscope, i.e., the ability to distinguish two separate particles, is limited by the Rayleigh criterion, sub-pixel accuracy in particle localization can be achieved through fitting the PSF of the particle, which is limited by the SNR. The accuracy and precision of various localization methods has been extensively reviewed,[186,262,263] so a brief explanation of commonly used methods will be described below.

Centroid calculation: Finding centroids involves locating the all local brightness maxima in an image, which correspond to potential particles.[20] The intensity-weighted centroid, similar to a center of mass calculation, is used to identify the particle position. Centroid fitting is one of the fastest methods of localizing particles, which makes it attractive to researchers.

Gaussian Fit: As described previously, for a diffraction limited probe the brightness intensity profile can be described as an Airy disk whose center spot can be approximated as a 2D Gaussian,

$$G(x, y) = A^*\exp\left[-\frac{(x - x_0)^2 + (y - y_0)^2}{B}\right]. \quad (6)$$

Parameters of the Gaussian function can be determined through non linear least-squares minimization[264] or maximum likelihood estimation.[265] Due to the iterative nature of these algorithms, they can be computationally expensive and time intensive, particularly for images with a high concentration of particles. However, at moderate and high SNRs these fitting methods are more precise than centroid fitting, making them ideal for high precision particle tracking. At low SNR, SNR < 3, the localization error of centroid and Gaussian fitting are comparable.[186]

Radially symmetry-based tracking: Without optical aberrations, the PSF of a particle is generally radially symmetric. Parthasarathy[186] has developed an algorithm that utilizes the radially symmetric nature of the particle intensity to achieve sub-pixel accuracy. At all SNRs, radial symmetry is comparable to or exceeds

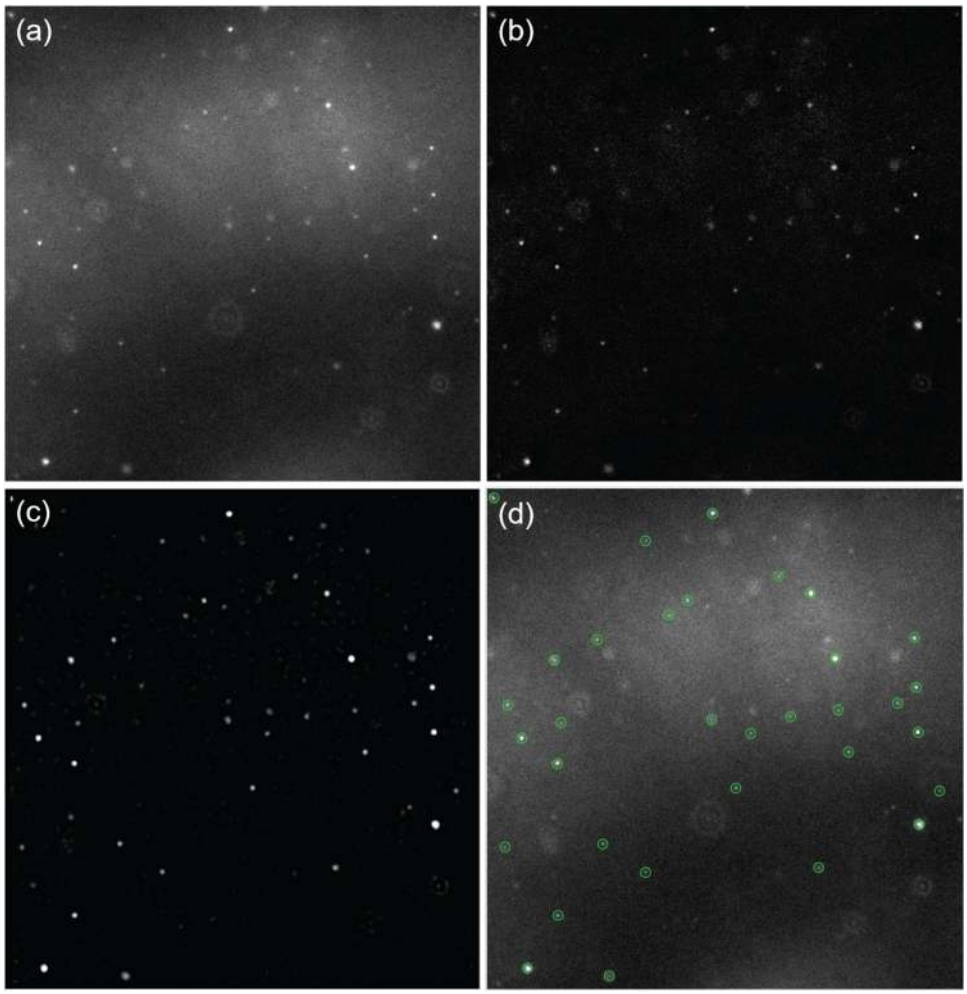

FIG. 4. (a) Raw image of diffusing nanoparticles during video acquisition. (b) Enhanced images after removing nonuniform background. (c) Image after applying a bandpass filter with a user inputted size criterion. (d) Localization of particles (green circles) with user inputted threshold and size criterion overlaid on the original, unedited image. Particles are CdSe/CdS quantum dots functionalized with a poly(ethylene glycol) brush, hydrodynamic diameter 10 nm.

Gaussian fitting in precision, but due to the non-iterative nature of the algorithm, the calculation time is substantially less; the algorithm localizes particles 100× faster than its Gaussian fitting counterpart.[186] The decrease in computational time coupled with high precision makes this algorithm ideal for nanoscale particle tracking. Furthermore, for microscopy methods where intensity obeys superposition, this method provides superior results when multiple particle images overlap slightly, useful in systems where particle density is high.[266]

3. Filtering unwanted particles

Localization algorithms often pick up on potential particles that do not correspond to real particles, whether they are local intensity maxima from camera noise or non-uniform background contributions that were not successfully removed during image preprocessing. Identifying proper user defined threshold parameters during image processing such as a minimum particle size (particle identification), an approximate full-width-half-maximum of the Airy disk (particle localization), and a minimum brightness threshold (particle identification) can help eliminate many false particle identifications. Additionally, random camera errors in the form of intensity fluctuations are rarely constant in subsequent frames, and can be eliminated by requiring a minimum number of successive frames for a particle trajectory.[20]

4. Tracking the path of individual particles

Once the positions of particles are established, particle trajectories are determined by linking particle positions between successive frames. For particles exhibiting Brownian motion, there is no preferential direction of motion; therefore, trajectories cannot be calculated by methods that utilize expected particle position and velocity. Proximity of particles between successive frames is the best method to track a single object between multiple frames, and is utilized in most particle tracking software.[20] To do this effectively, a maximum threshold distance of a single particle, larger than the distance traveled by a particle in a single frame, should be identified. A substantial limitation of this common method of linking particle trajectories is that it is only successful if the

experiment is conducted such that probe concentration is fairly sparse. If the maximum distance traveled is more than the interparticle distance of two neighboring particles, particle positions can be improperly linked resulting in false trajectories. For high particle density systems where nearest-neighbor tracking fails, multiple hypothesis tracking has been implemented successfully, though it is computationally expensive.[267,268]

V. PARTICLE TRACKING ANALYSIS

A. Mean squared displacement (MSD)

The mean squared displacement (MSD) of a particle, or the square of the net distance a particle travels, is described by

$$MSD(\tau) = \langle \Delta r(\tau)^2 \rangle_t = \langle [r(t+\tau) - r(t)]^2 \rangle_t, \tag{7}$$

where τ is the lag time, $r(t)$ is the position of the particle at absolute time t, and $\langle \rangle_t$ denotes the averaging over time.

Although calculating MSD from a particle trajectory seems straightforward, there are many considerations one should take into account to obtain and evaluate the robustness of MSDs. Consider a trajectory of a particle at N discreet time points and with time steps of Δt. To measure the MSD at $\tau = n\Delta t$ one could use an ensemble of $m = N/n$ completely uncorrelated displacement events of $\Delta r_i = r[(i+1)n\Delta t] - r[i\,n\Delta t]$, where

$$\langle \Delta r(\tau)^2 \rangle = \frac{1}{m} \sum_{i=1}^{m} \Delta r_i^2. \tag{8}$$

For this ensemble, the standard error in calculated MSD is estimated as $e_{MSD} = \frac{1}{\sqrt{m}} \langle \Delta r(\tau)^2 \rangle$. One could also decide to use all of the available $N - n$ displacement events of $\Delta r_i = r[(i+n)\Delta t] - r[(i\Delta t]$ and calculate the MSD from

$$\langle \Delta r(\tau)^2 \rangle = \frac{1}{N-n} \sum_{i=1}^{N-n} \Delta r_i^2. \tag{9}$$

However, in this method, because multiple displacement vectors are taken from oversampling sub-trajectories of a particle, displacement vectors are not fully uncorrelated and above equation for e_{MSD} cannot be used to evaluate the standard error in MSD. Nevertheless, this overcounting yields higher statistical power than single counting and is advisable specially when the number of data points is limited. For this method, the standard error is roughly $e_{MSD} = \frac{1}{\sqrt{2m}} \langle \Delta r(\tau)^2 \rangle$.

The diffusive motion of tracers embedded in soft materials often is utilized to probe their complex viscoelastic responses through the fluctuation dissipation theorem. In this technique which is referred to as microrheology, the MSD of the particle is related to the frequency dependent shear modulus of the materials via the Generalized Stokes–Einstein Relation (GSER)

$$G(s) = \frac{k_B T}{\pi a s \tilde{MSD}(s)}, \tag{10}$$

where $G(s)$ is the shear modulus and $\tilde{MSD}(s)$ is the Laplace transform of the MSD. In contrast to the bulk rheology, microrheology can be accomplished on small sample volumes and probes the local rheology of soft materials, and has been reviewed extensively by others.[1–3]

A wide variety of errors can disrupt the accuracy of the MSD if unaccounted for. These errors often are confused as physically significant since they generate features in MSDs that mimic subdiffusive or superdiffusive behavior. Sections V A 1–V A 5 discuss error sources that are often inevitable in particle tracking, detailing their individual effects on MSDs to prevent misidentifying them as physically relevant contributions to particle motion or mechanics of the surrounding medium. The effects of these errors on an ensemble MSD can be viewed in Fig. 5(a).

1. Static error

Static error results from the instrument's capability to locate a particle and is dependent on the construction of the microscope and random error. To quantify static error, particles can be immobilized in either in a highly cross-linked gel, epoxy, or by attaching or allowing particles to settle onto a cover slip. If the particles are immobile, then the position of the particle is theoretically constant.

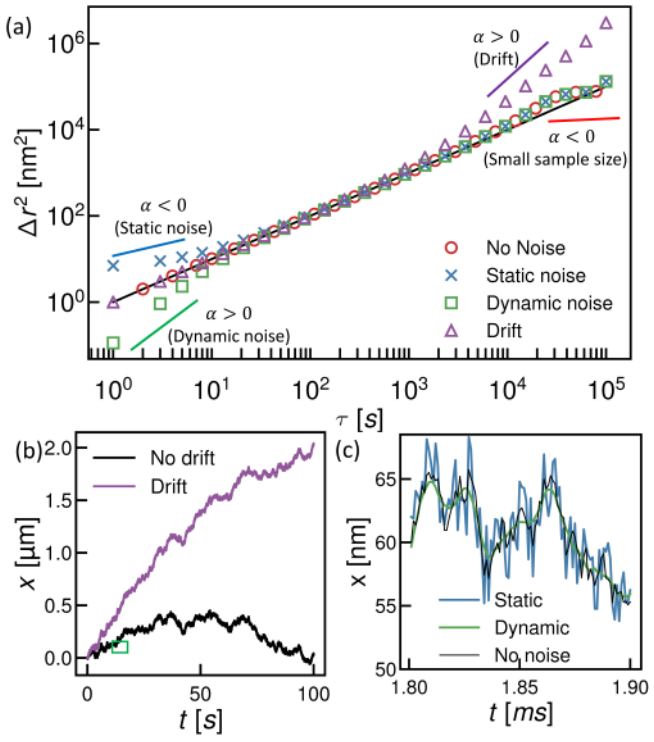

FIG. 5. (a) MSD of a simulated 1D trajectory of particle with Brownian diffusive motion, black line. Symbols show MSDs of the same trajectory with numerically introduced errors. (b) Trajectory of particle over time, black line, and the same trajectory with added drift. (c) Trajectory of the particle convoluted with static error (blue line) and dynamic error (green line).

However, random error including camera noise, thermal fluctuations of the microscope, and vibrations can contribute to measured particle motion creating a non-zero noise term. The measured motion of these immobilized particles is defined as the static error. Ideally, experiments performed to quantify the static error should be conducted under similar imaging conditions to those used in experiments, especially similar SNRs. Alternatively, Gaussian random numbers can be added to each pixel with an amplitude corresponding to the camera noise, and the resulting position shifts are measured. The RMS of these shifts is the static error.

Static error will always cause the measured MSD to be larger than that of the physical MSD, since the presence of position error increases the measured displacement [Fig. 5(c)] and, therefore, the MSD. Since at short lag times, the physical MSD is the smallest, the effect of static noise is more evident in this regime. For instance, for the particle diffusing randomly in a viscous fluid, the MSD will be affected by static noise as

$$\langle \Delta x^2 \rangle_{measured} = \langle \Delta x^2 \rangle_{physical} + 2\sigma_x^2, \tag{11}$$

where σ_x is the standard deviation of the static error.[253] As plotted in Fig. 5(a), the MSD of such a particle in the short lag times shows a subdiffusive trend if the probe motion is smaller or similar to the precision of the MSD. One approach to correct the MSD is to subtract $2\sigma_x^2$ from it and use the estimated error to determine at what point the result is insignificant. For a particle moving with an anomalous diffusion process, the effect of static noise in MSD is more complicated.[253] Therefore, prior to any particle tracking experiment, the static noise level should be determined.

2. Dynamic error

Dynamic error arises from the movement of a particle during a finite exposure time. If a particle moves substantially during a given exposure, localization algorithms will give a time-averaged position for the exposure rather than the absolute position [Fig. 5(c)].[253] Ideally, this error would be minimized with decreasing exposure time. However, short exposure time without increasing the brightness of the particles leads to a decrease in spatial accuracy during localization.[19] The tradeoff between spatial accuracy and dynamic error is something one must consider, particularly when the goal is high precision tracking. Similar to static noise, dynamic noise also alters the MSD in short lag times. While static noise artificially increases the particle MSD at short lag times, dynamic error decreases the measured MSD compared to the actual MSD, generating artifacts of superdiffusive behavior as the full particle path cannot be adequately described by the series of positions captured [Fig. 5(a)]. Dynamic error and static error, and, therefore, their contributions to the MSD, can be decreased with proper microscope parameters, as described in Sec. IV.

3. Drift

As mentioned previously, sample drift can cause substantial error during the length scale of the experiment. To remove the effect of drift that is constant in time and across the field of view, we can use $MSD' = MSD - (\Delta x\tau)^2$, where Δx is the constant drift displacement between consecutive frames. Ideally, it is best to eliminate sources of drift during sample fabrication. If possible, the sample chamber should be sealed and the microscope chamber isolated. The sample chamber should also settle on the stage to allow for any thermal relaxations and the flow due to the movement of the chamber stop. However, if the drift is still present, it can be corrected during post tracking analysis by "detrending" particle tracks. In a system without drift, particle motion is randomly and isotropically oriented, but a constant source of drift will introduce directionality to particle motion [Fig. 5(b)]. At long lag times, this creates artificial superdiffusive behavior in the particle MSD as shown in Fig. 5(a). If there are a large number of particles in the field of view, then the instantaneous drift displacement, $\Delta r^d(t)$, at each time step can be determined by calculating the average displacement of all particles,

$$\Delta r^d(t = n\Delta t) = \frac{1}{N}\sum_i^N r_i(t + \Delta t) - r_i(t), \tag{12}$$

where i is indices of particles, and Δt is the time between two consecutive frames. The total drift displacement at time $t = n\Delta t$ is $r^d(t) = \sum_q^n \Delta r^d(q\Delta t)$. The trajectories of each particle then could be modified by subtracting $r^d(t)$ from each individual trajectory. However, if the drift is spatially heterogeneous, subtracting the average motion of particles is not appropriate. The subtraction of drift from individual particle tracks has been achieved through the use of maximum likelihood estimation[269] or by limiting analysis to motion orthogonal to the suspected drift direction[270] in cases where drift cannot be removed, though best practice is to remove drift through a proper microscope and sample isolation when possible.

4. Pixel biasing

Special consideration must be taken when localizing particles to sub-pixel accuracy, as certain systematic errors can be introduced. Namely, there is a risk of "pixel biasing," where the particle localization algorithm records the position of the particle to the nearest pixel rather than a sub-pixel value. This can be checked by examining the distribution of the fractional portion of the coordinates of the particles; if the histogram is flat, then there is no biasing toward the edge of pixels. However, if there is a noticeable minimum, this is indicative of the localization algorithm rounding to the nearest pixel and could introduce an error up to 0.5 pixels. This can occur due to poor selection of imaging parameters or improper tracking parameters. If the brightness from the probe only spans 1–2 pixels, the magnification is too low and pixel biasing is likely to occur. Additionally, image processing can result in pixel biasing if parameters for processing images and identifying particles are incorrect, such as inputting a predicted spot size that is too small which can cause the mask to prematurely truncate the intensity profile. This forces the edges of the intensity profile to zero prematurely, introducing pixel bias.[19]

5. Bias toward mobile particles

Another potential artifact of the ensemble MSD is related to the inherent bias for measuring slower moving particles. If some

particles are diffusing out of the field of view, either out of the x–y plane or in the z-direction, then at long lag times the MSD is dominated by the slower moving particles, as that subset of particles are most likely to stay within the field of view. This results in a downturn in the MSD curve at long lag times, when the particle displacement approaches the depth of focus [Fig. 5(a)]. This can be accounted for by only utilizing the portion of the MSD, where the MSD is below the square of the depth of focus.

B. van Hove distribution function

While MSD at different lag times reveals the dynamics of ensemble particle motion, the distribution of particle displacements carries more details about the heterogeneity and structure of materials. Conventionally, the van Hove distribution function $G(r, \tau)$ has been used for characterizing the spatial and temporal distributions of particles in a material.[271] In a general form, the van Hove distribution is a real-space dynamical correlation function that describes the probability of finding particle i at distance $r + \Delta r$ and time $t + \tau$, given that particle j is located at r at time t. This is described by the correlation equation,

$$G(\Delta r, \tau) = \frac{1}{N}\left\langle \sum_{i=1}^{N}\sum_{j=1}^{N} \delta(r_j(t) - r_i(t+\tau) - \Delta r)\right\rangle_t, \quad (13)$$

where δ indicates the Dirac delta function.

In the specific case that $\tau = 0$, the van Hove function reduces to the pair correlation function, $g(r)$. In the case where $i = j$, the van Hove takes the more familiar form of

$$G(\Delta r, \tau) = \frac{1}{N}\left\langle \sum_{i=1}^{N} \delta(r_i(t) - r_i(t+\tau) - \Delta r)\right\rangle_t, \quad (14)$$

which describes the motion of the particles. For the rest of the section, the term van Hove distribution will represent this form of Eq. (13) which often is referred to as the "self "portion of the van Hove distribution.[272]

For identical particles (diameter, surface chemistry) in a homogeneous environment, the corresponding approximation for the self part of the van Hove function assumes a Gaussian shape

$$G(\Delta x, \tau) = \frac{1}{\sqrt{(2\pi)\sigma(\tau)}}\exp\left[-\frac{\Delta x^2}{2\sigma(\tau)^2}\right]. \quad (15)$$

If the particles are identical but experience different local environments, or the particles themselves are heterogeneous, the van Hove correlation function will deviate from the Gaussian functional form, as indicated by the emergence of long tails (Fig. 6). Although other functional forms, for example, the stable distribution, can be used to describe the non-Gaussian van-Hove, often the tail of distribution carries the physical signature of the particle motion. These tails can be fit with an exponential function, which provides a characteristic length for particle diffusion at a given τ.[4,5]

In order to generate a probability distribution of particle displacement at different lag times, proper sampling and binning methods should be chosen. As shown in Fig. 6, the probability of large displacement events in many random processes are small compared to those of small displacements. Therefore, regular methods for measuring histograms, such as uniform binning, are not the most suitable in determining a van Hove distribution, especially its tail. In the uniform binning method, the number of events at each interval with equal size is counted, and probability events measured. To prevent noisy histograms, one simple way is to generate non-uniform grids such as logarithmically uniform grids. Logarithmic binning is especially effective for van Hove distributions with exponential distributions and has been used to visualize probability distribution functions of power-law distributions.[273]

The other method to obtain a van Hove with equal statistical robustness at each point is to generate a histogram with an equal number of data points, N_{count}, in each bin. To generate such a histogram, the width of each bin, $s(x)$, varies based on the range of the points in the bin. The geometric mean of data points in each bin is computed as the location of the center bin, and the probability value of each bin is calculated as $P(x) = N_{count}/s(x)$. As an example, Fig. 7 shows how accurately the two different binning methods represent the probability distribution of the numerically generated random numbers with the stable distribution and exponential tails. When each bin has the same number of data points but different widths, the histogram overlaps with the expected distribution (red circles) in Fig. 7. The histogram with a uniform bin size, however, fails to predict the distribution.

C. Qualitatively and quantitatively measuring heterogeneity

One of the key advantages of particle tracking is the ability to distinguish distinct populations of diffusing particles thereby detecting heterogeneity in the system. Various groups have utilized different measures to detect and statistically distinguish different populations of particles. While not an exhaustive list of methods to identify the heterogeneity in particle dynamics and distinct populations in particle tracking data, the following methods are commonly used and are an excellent starting point for additional analysis.

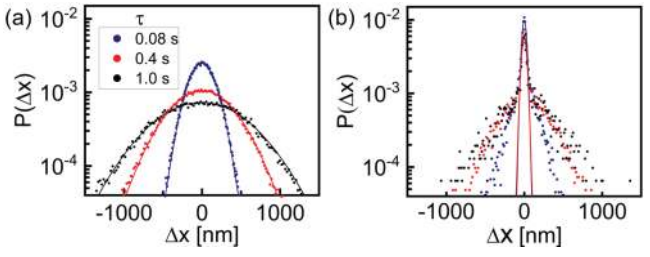

FIG. 6. van Hove correlation functions at a lag time, τ, of 0.08, 0.4, and 1.0 s for (a) nanoparticle diffusion in a homogeneous medium (glycerol:water) and (b) nanoparticle diffusion in a heterogeneous gel (polyacrylamide). Solid lines are Gaussian fits, with the emergence of exponential tails in (b) indicating deviations from Gaussian statistics. Particles are CdSe/CdS quantum dots functionalized with a poly(ethylene glycol) brush, hydrodynamic diameter 10 nm.

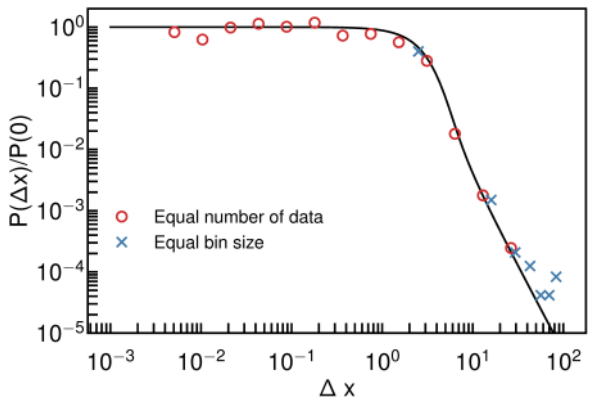

FIG. 7. van Hove for numerically generated random numbers with stable distribution shown with solid black line. Symbols show the probability of these numbers calculated by the equal bin size method (blue crosses) and by the method with an equal number of data in each bin (red circles).

One method to quantify heterogeneity is the non-Gaussianity parameter, NG_τ or α_2, which characterizes the deviation of the van Hove distribution from Gaussian behavior.[274] In short, the parameter compares the second and fourth moments of the displacements for each lag time, τ. The non-Gaussian parameter is described by the equation

$$NG_\tau = \frac{\langle \Delta x^4(\tau) \rangle}{3\langle \Delta x^2(\tau) \rangle^2} - 1. \tag{16}$$

By definition, if $NG_\tau = 0$ for each τ, then the displacement increments are Gaussian. Furthermore, if $NG_\tau \neq 0$ it suggests the presence of heterogeneity at the length scale of the probe particle displacement.[275] Furthermore, NG_τ can be used to investigate the evolution of apparent heterogeneity over increasing length scales. If $NG_\tau = 0$ at short τ, but drastically increases as at longer τ, then the non-Gaussian parameter can be used to characterize the heterogeneity the particle experiences as length scale dependent.[276] This is also described as the excess kurtosis of the van Hove correlation function, described as

$$ku = \frac{\sum_{i=1}^{n} (x_i - (\bar{x}))^4}{(n-1)\sigma^4} - 3, \tag{17}$$

where x is the mean and σ is the standard deviation of the distribution. A homogeneous environment corresponds to $ku = 0$, and deviating values of ku indicate heterogeneity. This was first used to quantify the distribution of environments felt by colloidal polystyrene spheres during gelation of hectorite suspensions, though it has also been subsequently used to characterize nanoparticle diffusion.[277]

A significant concern of measuring heterogeneity using particle tracking is the bias toward measuring mobile particles. As mobile particles move in and out of the focal plane, a large number of short, mobile tracks are created resulting in a bias toward more mobile particles at shorter τ when examining heterogeneity. Savin and Doyle[278] formulated a method that weights each trajectory proportional to its duration in time, eliminating the bias created by short mobile particle trajectories. The heterogeneity ratio, HR, is defined as

$$HR = \frac{M_2(\tau)}{M_1(\tau)^2}, \tag{18}$$

where $M_1(\tau)$ is the estimator for the weighted ensemble average, or the MSD weighted based on the duration of the trajectory, and $M_2(\tau)$ is its corresponding variance. As a reference, theoretical calculations indicate that HR for a water, a homogeneous Newtonian fluid solution, is approximately 0.6. Increasing heterogeneity, studied by Doyle and co-workers via the gelation of Laponite solutions, resulted in increased values of HR, with HR 1.75 at peak heterogeneity.[279]

To further quantify the statistical significance of heterogeneity, different populations of diffusing particles can be sorted into statistically distinct bins. This has been done for particle tracking using the F-statistic,

$$f_{l,k} = \frac{\sigma_k^2/n_k}{\sigma_l^2/n_l}, \tag{19}$$

where k and l correspond to the two independent, random, normally distributed quantities, with variance σ^2 and n degrees of freedom. The variances of these two distributions can be compared using the F test, which compares the two distributions using the F statistic, and determines if the two distributions are statistically different within a calculated confidence interval. Valentine and co-workers[280] utilized the F statistic and the F test to cluster individual particle tracks into statistically different clusters. They found that for a homogeneous environment, such as glycerol–water solutions, the F test returns only one cluster, since the particles experience the same local environment. For agarose gels, which are heavily heterogeneous, the F test indicated multiple statistically different clusters of particle motion at short lag times, indicating the presence of disparate microenvironments experienced by the particles.

VI. THE FUTURE OF PARTICLE TRACKING AND CONCLUSION

The future of particle tracking in part depends on the continued improvement of optical techniques, probe quality, and the advancement of data processing techniques. As researchers develop probes that resist photobleaching or are increasingly bright, we will be able to utilize them to visualize smaller and smaller length scales to increase our understanding of nanoprobe diffusion in complex environments. In data processing, machine learning offers promise in many phases of particle tracking including detection,[281,282] subpixel localization,[283,284] trajectory linking,[285] and trajectory analysis.[286–288] These advances have the potential to improve the performance, robustness, accuracy, and ease of use of particle tracking software, allowing this technique to reach more experimenters. However, users should take care when using networks trained with

simulated or other user experimental data, and check for the effects of training bias on their own results. Ultimately, facilitating users in modifying networks with their own data through open source software platforms will be essential to capitalizing on the full potential of machine learning in particle tracking.

Particle tracking is a robust method for determining the mobility of nanoparticles in a variety of soft matter systems. While other methods can produce useful dynamic information, particle tracking has been used to image particles and probes in heterogeneous environments, yielding structural and dynamic information inaccessible with ensemble average techniques. This tutorial highlighted key factors for conducting successful particle tracking experiments, including best practices for obtaining high quality data, detailing some of the more common algorithms used for localization and tracking, detailing data analysis, and identifying potential errors that can present in the measured diffusion profiles. With these tools, a wide variety of dynamic and structural questions related to nanoparticle and soft matter systems can be explored.

AUTHOR'S CONTRIBUTIONS

K. A. Rose and M. Molaei contributed equally to this work.

ACKNOWLEDGMENTS

Support was provided by NSF-PIRE-OISE-1545884 (R.J.C., D.L., and K.A.R.), a NSF Graduate Fellowship (K.A.R. and M.J.B.), NSF-POLYMERS-DMR-1905912 (R.J.C.), NSF-CBET-1706014 (R.J.C. and M.J.B.), ACS-PRF-55120-ND5 (M.M. and J.C.C.), and partial support from Penn PSOC-NIH-U54-CA193417 (M.M. and J.C.C.). Particle tracking experiments were performed at the Scanning and Local Probe Facility at the Singh Center for Nanotechnology at the University of Pennsylvania, supported by NSF-MRSEC-DMR-1720530. The authors would like to thank Dr. Christopher Murray for providing quantum dots, Dr. Yale Goldman for introducing TIRF and iSCAT to the authors, Dr. Matthew Caporizzo for advice regarding microscope assembly and data analysis, and Dr. Matthew Brukman for instrument support in the Singh Center for Nanotechnology.

REFERENCES

[1]P. Cicuta and A. M. Donald, "Microrheology: A review of the method and applications," Soft Matter **3**, 1449–1455 (2007).
[2]W. Liu and C. Wu, "Rheological study of soft matters: A review of microrheology and microrheometers," Macromol. Chem. Phys. **219**, 1700307 (2018).
[3]E. M. Furst and T. M. Squires, *Microrheology* (Oxford University Press, 2018).
[4]E. Parrish, M. A. Caporizzo, and R. J. Composto, "Network confinement and heterogeneity slows nanoparticle diffusion in polymer gels," J. Chem. Phys. **146**, 203318 (2017).
[5]C. H. Lee, A. J. Crosby, T. Emrick, and R. C. Hayward, "Characterization of heterogeneous polyacrylamide hydrogels by tracking of single quantum dots," Macromolecules **47**, 741–749 (2014).
[6]E. Parrish, K. A. Rose, M. Cargnello, C. B. Murray, D. Lee, and R. J. Composto, "Nanoparticle diffusion during gelation of tetra poly(ethylene glycol) provides insight into nanoscale structural evolution," Soft Matter **16**, 2256–2265 (2020).
[7]D. Bhatia, S. Arumugam, M. Nasilowski, H. Joshi, C. Wunder, V. Chambon, V. Prakash, C. Grazon, B. Nadal, P. K. Maiti, L. Johannes, B. Dubertret, and Y. Krishnan, "Quantum dot-loaded monofunctionalized DNA icosahedra for single-particle tracking of endocytic pathways," Nat. Nanotechnol. **11**, 1112–1119 (2016).
[8]H. Ewers, A. E. Smith, I. F. Sbalzarini, H. Lilie, P. Koumoutsakos, and A. Helenius, "Single-particle tracking of murine polyoma virus-like particles on live cells and artificial membranes," Proc. Natl. Acad. Sci. **102**, 15110–15115 (2005).
[9]M. E. Grady, E. Parrish, M. A. Caporizzo, S. C. Seeger, R. J. Composto, and D. M. Eckmann, "Intracellular nanoparticle dynamics affected by cytoskeletal integrity," Soft Matter **13**, 1873–1880 (2017).
[10]M. Kawai, H. Higuchi, M. Takeda, Y. Kobayashi, and N. Ohuchi, "Dynamics of different-sized solid-state nanocrystals as tracers for a drug-delivery system in the interstitium of a human tumor xenograft," Breast Cancer Res. **11**, R43 (2009).
[11]H. Tada, H. Higuchi, T. M. Wanatabe, and N. Ohuchi, "*In vivo* real-time tracking of single quantum dots conjugated with monoclonal anti-HER2 antibody in tumors of mice," Cancer Res. **67**, 1138–1144 (2007).
[12]R. J. Bloom, J. P. George, A. Celedon, S. X. Sun, and D. Wirtz, "Mapping local matrix remodeling induced by a migrating tumor cell using three-dimensional multiple-particle tracking," Biophys. J. **95**, 4077–4088 (2008).
[13]Y. Li, J. Schnekenburger, and M. H. G. Duits, "Intracellular particle tracking as a tool for tumor cell characterization," J. Biomed. Opt. **14**, 064005 (2009).
[14]M. Dawson, E. Krauland, D. Wirtz, and J. Hanes, "Transport of polymeric nanoparticle gene carriers in gastric mucus," Biotechnol. Prog. **20**, 851–857 (2004).
[15]K. Forier, A.-S. Messiaen, K. Raemdonck, H. Deschout, J. Rejman, F. De Baets, H. Nelis, S. C. De Smedt, J. Demeester, T. Coenye, and K. Braeckmans, "Transport of nanoparticles in cystic fibrosis sputum and bacterial biofilms by single-particle tracking microscopy," Nanomedicine **8**, 935–949 (2012).
[16]S. K. Lai, D. E. O'Hanlon, S. Harrold, S. T. Man, Y.-Y. Wang, R. Cone, and J. Hanes, "Rapid transport of large polymeric nanoparticles in fresh undiluted human mucus," Proc. Natl. Acad. Sci. U.S.A. **104**, 1482–1487 (2007).
[17]J. S. Suk, S. K. Lai, Y.-Y. Wang, L. M. Ensign, P. L. Zeitlin, M. P. Boyle, and J. Hanes, "The penetration of fresh undiluted sputum expectorated by cystic fibrosis patients by non-adhesive polymer nanoparticles," Biomaterials **30**, 2591–2597 (2009).
[18]M. J. Skaug and D. K. Schwartz, "Tracking nanoparticle diffusion in porous filtration media," Ind. Eng. Chem. Res. **54**, 4414–4419 (2015).
[19]J. C. Crocker and B. D. Hoffman, "Multiple-particle tracking and two-point microrheology in cells," in *Methods in Cell Biology*, Cell Mechanics Vol. 83 (Academic Press, 2007), pp. 141–178.
[20]J. C. Crocker and D. G. Grier, "Methods of digital video microscopy for colloidal studies," J. Colloid Interface Sci. **179**, 298–310 (1996).
[21]A. Einstein, *Investigations on the Theory of the Brownian Movement* (Courier Corporation, 1956).
[22]G. D. J. Phillies, "Translational diffusion coefficient of macroparticles in solvents of high viscosity," J. Phys. Chem. **85**, 2838–2843 (1981).
[23]T. H. Lin and G. D. J. Phillies, "Translational diffusion coefficient of a macroparticulate probe species in salt-free poly(acrylic acid)-water," J. Phys. Chem. **86**, 4073–4077 (1982).
[24]G. S. Ullmann, K. Ullmann, R. M. Lindner, and G. D. J. Phillies, "Probe diffusion of polystyrene latex spheres in polyethylene oxide-water," J. Phys. Chem. **89**, 692–700 (1985).
[25]Z. E. Dell and K. S. Schweizer, "Theory of localization and activated hopping of nanoparticles in cross-linked networks and entangled polymer melts," Macromolecules **47**, 405–414 (2014).
[26]C. A. Grabowski and A. Mukhopadhyay, "Size effect of nanoparticle diffusion in a polymer melt," Macromolecules **47**, 7238–7242 (2014).
[27]J. T. Kalathi, U. Yamamoto, K. S. Schweizer, G. S. Grest, and S. K. Kumar, "Nanoparticle diffusion in polymer nanocomposites," Phys. Rev. Lett. **112**, 108301 (2014).
[28]J. Liu, D. Cao, and L. Zhang, "Molecular dynamics study on nanoparticle diffusion in polymer melts: A test of the Stokes–Einstein law," J. Phys. Chem. C **112**, 6653–6661 (2008).

[29]A. Tuteja, M. E. Mackay, S. Narayanan, S. Asokan, and M. S. Wong, "Breakdown of the continuum Stokes-vv-Einstein relation for nanoparticle diffusion," Nano Lett. **7**, 1276–1281 (2007).
[30]U. Yamamoto and K. S. Schweizer, "Theory of nanoparticle diffusion in unentangled and entangled polymer melts," J. Chem. Phys. **135**, 224902 (2011).
[31]U. Yamamoto and K. S. Schweizer, "Spatially dependent relative diffusion of nanoparticles in polymer melts," J. Chem. Phys. **139**, 064907 (2013).
[32]U. Yamamoto and K. S. Schweizer, "Microscopic theory of the long-time diffusivity and intermediate-time anomalous transport of a nanoparticle in polymer melts," Macromolecules **48**, 152–163 (2015).
[33]F. B. Wyart and P. G. D. Gennes, "Viscosity at small scales in polymer melts," Eur. Phys. J. E **97**, 93–97 (2000).
[34]R. A. Omari, A. M. Aneese, C. A. Grabowski, and A. Mukhopadhyay, "Diffusion of nanoparticles in semidilute and entangled polymer solutions," J. Phys. Chem. B **113**, 8449–8452 (2009).
[35]P. Tong, X. Ye, B. J. Ackerson, and L. J. Fetters, "Sedimentation of colloidal particles through a polymer solution," Phys. Rev. Lett. **79**, 2363–2366 (1997).
[36]J. Won, C. Onyenemezu, W. G. Miller, and T. P. Lodge, "Diffusion of spheres in entangled polymer solutions: A return to Stokes-Einstein behavior," Macromolecules **27**, 7389–7396 (1994).
[37]I. Kohli and A. Mukhopadhyay, "Diffusion of nanoparticles in semidilute polymer solutions: Effect of different length scales," Macromolecules **45**, 6143–6149 (2012).
[38]R. Poling-Skutvik, R. Krishnamoorti, and J. C. Conrad, "Size-dependent dynamics of nanoparticles in unentangled polyelectrolyte solutions," ACS Macro Lett. **4**, 1169–1173 (2015).
[39]F. Babaye Khorasani, R. Poling-Skutvik, R. Krishnamoorti, and J. C. Conrad, "Mobility of nanoparticles in semidilute polyelectrolyte solutions," Macromolecules **47**, 5328–5333 (2014).
[40]C. A. Grabowski, B. Adhikary, and A. Mukhopadhyay, "Dynamics of gold nanoparticles in a polymer melt," Appl. Phys. Lett. **94**, 021903 (2009).
[41]J. Choi, M. Cargnello, C. B. Murray, N. Clarke, K. I. Winey, and R. J. Composto, "Fast nanorod diffusion through entangled polymer melts," ACS Macro Lett. **4**, 952–956 (2015).
[42]L.-H. Cai, S. Panyukov, and M. Rubinstein, "Mobility of nonsticky nanoparticles in polymer liquids," Macromolecules **44**, 7853–7863 (2011).
[43]I. M. Tolić-Nørrelykke, E.-L. Munteanu, G. Thon, L. Oddershede, and K. Berg-Sørensen, "Anomalous diffusion in living yeast cells," Phys. Rev. Lett. **93**, 078102 (2004).
[44]I. Y. Wong, M. L. Gardel, D. R. Reichman, E. R. Weeks, M. T. Valentine, A. R. Bausch, and D. A. Weitz, "Anomalous diffusion probes microstructure dynamics of entangled F-actin networks," Phys. Rev. Lett. **92**, 178101 (2004).
[45]L.-H. Cai, S. Panyukov, and M. Rubinstein, "Hopping diffusion of nanoparticles in polymer matrices," Macromolecules **48**, 847–862 (2015).
[46]P. J. Griffin, V. Bocharova, L. R. Middleton, R. J. Composto, N. Clarke, K. S. Schweizer, and K. I. Winey, "Influence of the bound polymer layer on nanoparticle diffusion in polymer melts," ACS Macro Lett. **5**, 1141–1145 (2016).
[47]C.-C. Lin, P. J. Griffin, H. Chao, M. J. A. Hore, K. Ohno, N. Clarke, R. A. Riggleman, K. I. Winey, and R. J. Composto, "Grafted polymer chains suppress nanoparticle diffusion in athermal polymer melts," J. Chem. Phys. **146**, 203332 (2017).
[48]P. Malo de Molina, S. Lad, and M. E. Helgeson, "Heterogeneity and its influence on the properties of difunctional poly(ethylene glycol) hydrogels: Structure and mechanics," Macromolecules **48**, 5402–5411 (2015).
[49]B. G. Bush, J. M. Shapiro, F. W. DelRio, R. F. Cook, and M. L. Oyen, "Mechanical measurements of heterogeneity and length scale effects in PEG-based hydrogels," Soft Matter **11**, 7191–7200 (2015).
[50]O. Lieleg, I. Vladescu, and K. Ribbeck, "Characterization of particle translocation through mucin hydrogels," Biophys. J. **98**, 1782–1789 (2010).
[51]B. S. Schuster, D. B. Allan, J. C. Kays, J. Hanes, and R. L. Leheny, "Photoactivatable fluorescent probes reveal heterogeneous nanoparticle permeation through biological gels at multiple scales," J. Control. Release. **260**, 124–133 (2017).
[52]A. Honigmann, V. Mueller, H. Ta, A. Schoenle, E. Sezgin, S. W. Hell, and C. Eggeling, "Scanning STED-FCS reveals spatiotemporal heterogeneity of lipid interaction in the plasma membrane of living cells," Nat. Commun. **5**, 5412 (2014).
[53]P. Sengupta, T. Jovanovic-Talisman, D. Skoko, M. Renz, S. L. Veatch, and J. Lippincott-Schwartz, "Probing protein heterogeneity in the plasma membrane using PALM and pair correlation analysis," Nat. Methods **8**, 969–975 (2011).
[54]D. Lingwood, H.-J. Kaiser, I. Levental, and K. Simons, "Lipid rafts as functional heterogeneity in cell membranes," Biochem. Soc. Trans. **37**, 955–960 (2009).
[55]P. S. Stewart, R. Murga, R. Srinivasan, and D. de Beer, "Biofilm structural heterogeneity visualized by three microscopic methods," Water Res. **29**, 2006–2009 (1995).
[56]E. Guiot, P. Georges, A. Brun, M. P. Fontaine-Aupart, M. N. Bellon-Fontaine, and R. Briandet, "Heterogeneity of diffusion inside microbial biofilms determined by fluorescence correlation spectroscopy under two-photon excitation," Photochem. Photobiol. **75**, 570–578 (2002).
[57]J. Wimpenny, W. Manz, and U. Szewzyk, "Heterogeneity in biofilms: Table 1," FEMS Microbiol. Rev. **24**, 661–671 (2000).
[58]P. S. Stewart and M. J. Franklin, "Physiological heterogeneity in biofilms," Nat. Rev. Microbiol. **6**, 199–210 (2008).
[59]E. Livneh, R. Prywes, S. Felder, Z. Kam, and J. Schlessinger, "Large deletions in the cytoplasmic kinase domain of the epidermal growth factor receptor do not affect its laternal mobility," J. Cell Biol. **103**, 327–331 (1986).
[60]W. L. C. Vaz, M. Criado, V. M. C. Madeira, G. Schoellmann, and T. M. Jovin, "Size dependence of the translational diffusion of large integral membrane proteins in liquid-crystalline phase lipid bilayers. A study using fluorescence recovery after photobleaching," Biochemistry **21**, 5608–5612 (1982).
[61]M. Edidin, M. C. Zúñiga, and M. P. Sheetz, "Truncation mutants define and locate cytoplasmic barriers to lateral mobility of membrane glycoproteins," Proc. Natl. Acad. Sci. U.S.A. **91**, 3378–3382 (1994).
[62]L. Salomé, J.-L. Cazeils, A. Lopez, and J.-F. Tocanne, "Characterization of membrane domains by frap experiments at variable observation areas," Eur. Biophys. J. **27**, 391–402 (1998).
[63]E. A. Reits, A. M. Benham, B. Plougastel, J. Neefjes, and J. Trowsdale, "Dynamics of proteasome distribution in living cells," EMBO J. **16**, 6087–6094 (1997).
[64]H. Pin-Kao, J. R. Abney, and A. Verkman, "Determinants of the translational mobility of a small solute in cell cytoplasm," J. Cell. Biol. **120**, 175–184 (1993).
[65]R. Swaminathan, S. Bicknese, N. Periasamy, and A. S. Verkman, "Cytoplasmic viscosity near the cell plasma membrane: Translational diffusion of a small fluorescent solute measured by total internal reflection-fluorescence photobleaching recovery," Biophys. J. **71**, 1140–1151 (1996).
[66]A. Partikian, B. Ölveczky, R. Swaminathan, Y. Li, and A. Verkman, "Rapid diffusion of Green fluorescent protein in the mitochondrial matrix," J. Cell. Biol. **140**, 821–829 (1998).
[67]R. D. Phair and T. Misteli, "High mobility of proteins in the mammalian cell nucleus," Nature **404**, 604–609 (2000).
[68]D. Marguet, E. T. Spiliotis, T. Pentcheva, M. Lebowitz, J. Schneck, and M. Edidin, "Lateral diffusion of GFP-tagged H2Ld molecules and of GFP-TAP1 reports on the assembly and retention of these molecules in the endoplasmic reticulum," Immunity **11**, 231–240 (1999).
[69]C. Vasudevan, W. Han, Y. Tan, Y. Nie, D. Li, K. Shome, S. C. Watkins, E. S. Levitan, and G. Romero, "The distribution and translocation of the G protein ADP-ribosylation factor 1 in live cells is determined by its GTPase activity," J. Cell Sci. **111**, 1277–1285 (1998).
[70]H. Yokoe and T. Meyer, "Spatial dynamics of GFP-tagged proteins investigated by local fluorescence enhancement," Nat. Biotechnol. **14**, 1252–1256 (1996).
[71]E. A. J. Reits, J. C. Vos, M. Grommé, and J. Neefjes, "The major substrates for TAP *in vivo* are derived from newly synthesized proteins," Nature **404**, 774–778 (2000).
[72]F. Waharte, K. Steenkeste, R. Briandet, and M.-P. Fontaine-Aupart, "Diffusion measurements inside biofilms by image-based fluorescence recovery after

photobleaching (FRAP) analysis with a commercial confocal laser scanning microscope," Appl. Environ. Microbiol. **76**, 5860–5869 (2010).
[73]J. D. Bryers and F. Drummond, "Local macromolecule diffusion coefficients in structurally non-uniform bacterial biofilms using fluorescence recovery after photobleaching (FRAP)," Biotechnol. Bioeng. **60**, 462–473 (1998).
[74]J. Korlach, P. Schwille, W. W. Webb, and G. W. Feigenson, "Characterization of lipid bilayer phases by confocal microscopy and fluorescence correlation spectroscopy," Proc. Natl. Acad. Sci. U.S.A. **96**, 8461–8466 (1999).
[75]P. Schwille, J. Korlach, and W. W. Webb, "Fluorescence correlation spectroscopy with single-molecule sensitivity on cell and model membranes," Cytometry **36**, 176–182 (1999).
[76]P. Schwille, U. Haupts, S. Maiti, and W. W. Webb, "Molecular dynamics in living cells observed by fluorescence correlation spectroscopy with one- and two-photon excitation," Biophys. J. **77**, 2251–2265 (1999).
[77]J. Ries, S. Chiantia, and P. Schwille, "Accurate determination of membrane dynamics with line-scan FCS," Biophys. J. **96**, 1999–2008 (2009).
[78]Q. Ruan, Y. Chen, E. Gratton, M. Glaser, and W. W. Mantulin, "Cellular characterization of adenylate kinase and its isoform: Two-photon excitation fluorescence imaging and fluorescence correlation spectroscopy," Biophys. J. **83**, 3177–3187 (2002).
[79]C. Fradin, A. Abu-Arish, R. Granek, and M. Elbaum, "Fluorescence correlation spectroscopy close to a fluctuating membrane," Biophys. J. **84**, 2005–2020 (2003).
[80]Y. Nomura, H. Tanaka, L. Poellinger, F. Higashino, and M. Kinjo, "Monitoring of *in vitro* and *in vivo* translation of green fluorescent protein and its fusion proteins by fluorescence correlation spectroscopy," Cytometry **44**, 1–6 (2001).
[81]K. Rippe, "Simultaneous binding of two DNA duplexes to the NtrC-enhancer complex studied by two-color fluorescence cross-correlation spectroscopy†," Biochemistry **39**, 2131–2139 (2000).
[82]S. Nath, J. Meuvis, J. Hendrix, S. A. Carl, and Y. Engelborghs, "Early aggregation steps in α-synuclein as measured by FCS and FRET: Evidence for a contagious conformational change," Biophys. J. **98**, 1302–1311 (2010).
[83]A. Pabbathi, S. Ghosh, and A. Samanta, "FCS study of the structural stability of lysozyme in the presence of morpholinium salts," J. Phys. Chem. B **117**, 16587–16593 (2013).
[84]M. Pitschke, R. Prior, M. Haupt, and D. Riesner, "Detection of single amyloid β-protein aggregates in the cerebrospinal fluid of Alzheimer's patients by fluorescence correlation spectroscopy," Nat. Med. **4**, 832–834 (1998).
[85]P. W. Wiseman, J. A. Squier, M. H. Ellisman, and K. R. Wilson, "Two-photon image correlation spectroscopy and image cross-correlation spectroscopy," J. Microsc. **200**, 14–25 (2000).
[86]N. O. Petersen, P. L. Höddelius, P. W. Wiseman, O. Seger, and K. E. Magnusson, "Quantitation of membrane receptor distributions by image correlation spectroscopy: Concept and application," Biophys. J. **65**, 1135–1146 (1993).
[87]N. O. Petersen, C. Brown, A. Kaminski, J. Rocheleau, M. Srivastava, and P. W. Wiseman, "Analysis of membrane protein cluster densities and sizes *in situ* by image correlation spectroscopy," Faraday Discuss. **111**, 289–305 (1999).
[88]M. A. Digman, P. W. Wiseman, A. R. Horwitz, and E. Gratton, "Detecting protein complexes in living cells from laser scanning confocal image sequences by the cross correlation raster image spectroscopy method," Biophys. J. **96**, 707–716 (2009).
[89]R. Pecora, "Dynamic light scattering measurement of nanometer particles in liquids," J. Nanopart. Res. **2**, 123–131 (2000).
[90]B. Chu and T. Liu, "Characterization of nanoparticles by scattering techniques," J. Nanopart. Res. **2**, 29–41 (2000).
[91]K. Schmitz, *Introduction to Dynamic Light Scattering by Macromolecules* (Elsevier, 1990).
[92]H. Holthoff, S. U. Egelhaaf, M. Borkovec, P. Schurtenberger, and H. Sticher, "Coagulation rate measurements of colloidal particles by simultaneous static and dynamic light scattering," Langmuir **12**, 5541–5549 (1996).
[93]E. Tombácz, G. Filipcsei, M. Szekeres, and Z. Gingl, "Particle aggregation in complex aquatic systems," Colloids Surf. A Physicochem. Eng. Aspects **151**, 233–244 (1999).
[94]I. Szilagyi, T. Szabo, A. Desert, G. Trefalt, T. Oncsik, and M. Borkovec, "Particle aggregation mechanisms in ionic liquids," Phys. Chem. Chem. Phys. **16**, 9515–9524 (2014).
[95]R. A. French, A. R. Jacobson, B. Kim, S. L. Isley, R. L. Penn, and P. C. Baveye, "Influence of ionic strength, pH, and cation valence on aggregation kinetics of titanium dioxide nanoparticles," Environ. Sci. Technol. **43**, 1354–1359 (2009).
[96]Y. T. He, J. Wan, and T. Tokunaga, "Kinetic stability of hematite nanoparticles: The effect of particle sizes," J. Nanopart. Res. **10**, 321–332 (2008).
[97]D. Chicea, "Nanoparticles and nanoparticle aggregates sizing by DLS and AFM," Optoelectronics Adv. Mater. **4**, 1210–1315 (2010).
[98]G. Brambilla, D. El Masri, M. Pierno, L. Berthier, L. Cipelletti, G. Petekidis, and A. B. Schofield, "Probing the equilibrium dynamics of colloidal hard spheres above the mode-coupling glass transition," Phys. Rev. Lett. **102**, 085703 (2009).
[99]L. Ramos and L. Cipelletti, "Ultraslow dynamics and stress relaxation in the aging of a soft glassy system," Phys. Rev. Lett. **87**, 245503 (2001).
[100]L. Cipelletti, S. Manley, R. C. Ball, and D. A. Weitz, "Universal aging features in the restructuring of fractal colloidal gels," Phys. Rev. Lett. **84**, 2275–2278 (2000).
[101]H. Guo, G. Bourret, R. B. Lennox, M. Sutton, J. L. Harden, and R. L. Leheny, "Entanglement-controlled subdiffusion of nanoparticles within concentrated polymer solutions," Phys. Rev. Lett. **109**, 055901 (2012).
[102]P. Nath, R. Mangal, F. Kohle, S. Choudhury, S. Narayanan, U. Wiesner, and L. A. Archer, "Dynamics of nanoparticles in entangled polymer solutions," Langmuir **34**, 241–249 (2018).
[103]R. Poling-Skutvik, K. I. S. Mongcopa, A. Faraone, S. Narayanan, J. C. Conrad, and R. Krishnamoorti, "Structure and dynamics of interacting nanoparticles in semidilute polymer solutions," Macromolecules **49**, 6568–6577 (2016).
[104]J. Lee, A. Grein-Iankovski, S. Narayanan, and R. L. Leheny, "Nanorod mobility within entangled wormlike micelle solutions," Macromolecules **50**, 406–415 (2017).
[105]R. Poling-Skutvik, A. H. Slim, S. Narayanan, J. C. Conrad, and R. Krishnamoorti, "Soft interactions modify the diffusive dynamics of polymer-grafted nanoparticles in solutions of free polymer," ACS Macro Lett. **8**, 917–922 (2019).
[106]S. Liu, E. Senses, Y. Jiao, S. Narayanan, and P. Akcora, "Structure and entanglement factors on dynamics of polymer-grafted nanoparticles," ACS Macro Lett. **5**, 569–573 (2016).
[107]Y. Shinohara, H. Kishimoto, N. Yagi, and Y. Amemiya, "Microscopic observation of aging of silica particles in unvulcanized rubber," Macromolecules **43**, 9480–9487 (2010).
[108]D. Pontoni, T. Narayanan, J.-M. Petit, G. Grübel, and D. Beysens, "Microstructure and dynamics near an attractive colloidal glass transition," Phys. Rev. Lett. **90**, 188301 (2003).
[109]R. Poling-Skutvik, R. C. Roberts, A. H. Slim, S. Narayanan, R. Krishnamoorti, J. C. Palmer, and J. C. Conrad, "Structure dominates localization of tracers within aging nanoparticle glasses," J. Phys. Chem. Lett. **10**, 1784–1789 (2019).
[110]F. A. d. M. Marques, R. Angelini, E. Zaccarelli, B. Farago, B. Ruta, G. Ruocco, and B. Ruzicka, "Structural and microscopic relaxations in a colloidal glass," Soft Matter **11**, 466–471 (2015).
[111]L. G. Wilson, V. A. Martinez, J. Schwarz-Linek, J. Tailleur, G. Bryant, P. N. Pusey, and W. C. K. Poon, "Differential dynamic microscopy of bacterial motility," Phys. Rev. Lett. **106**, 018101 (2011).
[112]V. A. Martinez, R. Besseling, O. A. Croze, J. Tailleur, M. Reufer, J. Schwarz-Linek, L. G. Wilson, M. A. Bees, and W. C. K. Poon, "Differential dynamic microscopy: A high-throughput method for characterizing the motility of microorganisms," Biophys. J. **103**, 1637–1647 (2012).
[113]D. Germain, M. Leocmach, and T. Gibaud, "Differential dynamic microscopy to characterize Brownian motion and bacteria motility," Am. J. Phys. **84**, 202–210 (2016).
[114]M. Reufer, V. A. Martinez, P. Schurtenberger, and W. C. K. Poon, "Differential dynamic microscopy for anisotropic colloidal dynamics," Langmuir **28**, 4618–4624 (2012).
[115]F. Giavazzi, C. Haro-Pérez, and R. Cerbino, "Simultaneous characterization of rotational and translational diffusion of optically anisotropic particles by optical microscopy," J. Phys. Condens. Matter **28**, 195201 (2016).

[116]M. S. Safari, R. Poling-Skutvik, P. G. Vekilov, and J. C. Conrad, "Differential dynamic microscopy of bidisperse colloidal suspensions," Microgravity **3**, 1–8 (2017).
[117]F. Ferri, A. D'Angelo, M. Lee, A. Lotti, M. C. Pigazzini, K. Singh, and R. Cerbino, "Kinetics of colloidal fractal aggregation by differential dynamic microscopy," Eur. Phys. J. Spec. Top. **199**, 139–148 (2011).
[118]Y. Gao, J. Kim, and M. E. Helgeson, "Microdynamics and arrest of coarsening during spinodal decomposition in thermoreversible colloidal gels," Soft Matter **11**, 6360–6370 (2015).
[119]E. J. Bailey, P. J. Griffin, R. J. Composto, and K. I. Winey, "Multiscale dynamics of small, attractive nanoparticles and entangled polymers in polymer nanocomposites," Macromolecules **52**, 2181–2188 (2019).
[120]B. Wang, S. M. Anthony, S. C. Bae, and S. Granick, "Anomalous yet Brownian," Proc. Natl. Acad. Sci. U.S.A. **106**, 15160–15164 (2009).
[121]E. Parrish, S. C. Seeger, and R. J. Composto, "Temperature-dependent nanoparticle dynamics in poly(*N*-isopropylacrylamide) gels," Macromolecules **51**, 3597–3607 (2018).
[122]A. Basset, P. Bouthemy, J. Boulanger, J. Salamero, and C. Kervrann, "Localization and classification of membrane dynamics in TIRF microscopy image sequences," in *2014 IEEE 11th International Symposium on Biomedical Imaging (ISBI)* (IEEE, 2014), pp. 830–833.
[123]A. Nenninger, G. Mastroianni, A. Robson, T. Lenn, Q. Xue, M. C. Leake, and C. W. Mullineaux, "Independent mobility of proteins and lipids in the plasma membrane of *Escherichia coli*," Mol. Microbiol. **92**, 1142–1153 (2014).
[124]Y. Sako, S. Minoghchi, and T. Yanagida, "Single-molecule imaging of EGFR signalling on the surface of living cells," Nat. Cell. Biol. **2**, 168–172 (2000).
[125]J. M. H. Goudsmits, A. M. van Oijen, and D. J. Slotboom, "Single-molecule fluorescence studies of membrane transporters using total internal reflection microscopy," in *Methods in Enzymology*, A Structure-Function Toolbox for Membrane Transporter and Channels Vol. 594, edited by C. Ziegler (Academic Press, 2017), pp. 101–121.
[126]S. M. Daly, T. M. Przybycien, and R. D. Tilton, "Adsorption of poly(ethylene glycol)-modified lysozyme to silica," Langmuir **21**, 1328–1337 (2005).
[127]S. G. Bike and D. C. Prieve, "Measurements of double-layer repulsion for slightly overlapping counterion clouds," Int. J. Multiphase Flow **16**, 727–740 (1990).
[128]C. Charlton, V. Gubala, R. P. Gandhiraman, J. Wiechecki, N. C. H. Le, C. Coyle, S. Daniels, B. D. MacCraith, and D. E. Williams, "TIRF microscopy as a screening method for non-specific binding on surfaces," J. Colloid Interface Sci. **354**, 405–409 (2011).
[129]R. Walder and D. K. Schwartz, "Dynamics of protein aggregation at the oil–water interface characterized by single molecule TIRF microscopy," Soft Matter **7**, 7616–7622 (2011).
[130]L. Xiao, L. Wei, C. Liu, Y. He, and E. S. Yeung, "Unsynchronized translational and rotational diffusion of nanocargo on a living cell membrane," Angew. Chem. Int. Ed. **51**, 4181–4184 (2012).
[131]G. Wang, W. Sun, Y. Luo, and N. Fang, "Resolving rotational motions of nano-objects in engineered environments and live cells with gold nanorods and differential interference contrast microscopy," J. Am. Chem. Soc. **132**, 16417–16422 (2010).
[132]P. Zhang, S. Lee, H. Yu, N. Fang, and S. H. Kang, "Super-resolution of fluorescence-free plasmonic nanoparticles using enhanced dark-field illumination based on wavelength-modulation," Sci. Rep. **5**, 1–9 (2015).
[133]L. Xiao and E. S. Yeung, "Optical imaging of individual plasmonic nanoparticles in biological samples," Ann. Rev. Anal. Chem. **7**, 89–111 (2014).
[134]C. Macias-Romero, M. E. P. Didier, V. Zubkovs, L. Delannoy, F. Dutto, A. Radenovic, and S. Roke, "Probing rotational and translational diffusion of nanodoublers in living cells on microsecond time scales," Nano Lett. **14**, 2552–2557 (2014).
[135]J. W. Ha, "Characteristic image patterns of single anisotropic plasmonic nanoparticles embedded in a gel matrix," Nanoscale **7**, 13159–13163 (2015).
[136]L. Starrs, W. C. K. Poon, D. J. Hibberd, and M. M. Robins, "Collapse of transient gels in colloid-polymer mixtures," J. Phys.: Condens. Matter **14**, 2485–2505 (2002).
[137]S. Spindler, J. Ehrig, K. König, T. Nowak, M. Piliarik, H. E. Stein, R. W. Taylor, E. Garanger, S. Lecommandoux, I. D. Alves, and V. Sandoghdar, "Visualization of lipids and proteins at high spatial and temporal resolution via interferometric scattering (iSCAT) microscopy," J. Phys. D: Appl. Phys. **49**, 274002 (2016).
[138]C.-L. Hsieh, S. Spindler, J. Ehrig, and V. Sandoghdar, "Tracking single particles on supported lipid membranes: Multimobility diffusion and nanoscopic confinement," J. Phys. Chem. B **118**, 1545–1554 (2014).
[139]D. Xu, Y. He, and E. S. Yeung, "Direct imaging of transmembrane dynamics of single nanoparticles with darkfield microscopy: Improved orientation tracking at cell sidewall," Anal. Chem. **86**, 3397–3404 (2014).
[140]D. Xu, Y. He, and E. S. Yeung, "Direct observation of the orientation dynamics of single protein-coated nanoparticles at liquid/solid interfaces," Angew. Chem. Int. Ed. Engl. **53**, 6951–6955 (2014).
[141]P. Kukura, H. Ewers, C. Müller, A. Renn, A. Helenius, and V. Sandoghdar, "High-speed nanoscopic tracking of the position and orientation of a single virus," Nat. Methods **6**, 923–927 (2009).
[142]A. Gemeinhardt, M. P. McDonald, K. König, M. Aigner, A. Mackensen, and V. Sandoghdar, "Label-free imaging of single proteins secreted from living cells via iSCAT microscopy," J. Vis. Exp. **141**, e58486 (2018).
[143]J. Andrecka, J. Ortega Arroyo, Y. Takagi, G. de Wit, A. Fineberg, L. MacKinnon, G. Young, J. R. Sellers, and P. Kukura, "Structural dynamics of myosin 5 during processive motion revealed by interferometric scattering microscopy," eLife **4**, e05413 (2015).
[144]K. M. Spillane, J. Ortega-Arroyo, G. de Wit, C. Eggeling, H. Ewers, M. I. Wallace, and P. Kukura, "High-speed single-particle tracking of GM1 in model membranes reveals anomalous diffusion due to interleaflet coupling and molecular pinning," Nano Lett. **14**, 5390–5397 (2014).
[145]G. de Wit, D. Albrecht, H. Ewers, and P. Kukura, "Revealing compartmentalized diffusion in living cells with interferometric scattering microscopy," Biophys. J. **114**, 2945–2950 (2018).
[146]D. Axelrod, D. Koppel, J. Schlessinger, E. Elson, and W. Webb, "Mobility measurement by analysis of fluorescence photobleaching recovery kinetics," Biophys. J. **16**, 1055–1069 (1976).
[147]D. Magde, E. Elson, and W. W. Webb, "Thermodynamic fluctuations in a reacting system—Measurement by fluorescence correlation spectroscopy," Phys. Rev. Lett. **29**, 705–708 (1972).
[148]E. L. Elson and D. Magde, "Fluorescence correlation spectroscopy. I. Conceptual basis and theory," Biopolymers **13**, 1–27 (1974).
[149]D. Magde, E. L. Elson, and W. W. Webb, "Fluorescence correlation spectroscopy. II. An experimental realization," Biopolymers **13**, 29–61 (1974).
[150]R. Pecora, "Quasi-elastic light scattering from macromolecules," Annu. Rev. Biophys. Bioeng. **1**, 257–276 (1972).
[151]S. B. Dierker, R. Pindak, R. M. Fleming, I. K. Robinson, and L. Berman, "X-ray photon correlation spectroscopy study of Brownian motion of gold colloids in glycerol," Phys. Rev. Lett. **75**, 449–452 (1995).
[152]R. Cerbino and V. Trappe, "Differential dynamic microscopy: Probing wave vector dependent dynamics with a microscope," Phys. Rev. Lett. **100**, 188102 (2008).
[153]R. J. Composto, R. M. Walters, and J. Genzer, "Application of ion scattering techniques to characterize polymer surfaces and interfaces," Mater. Sci. Eng. R Rep. **38**, 107–180 (2002).
[154]D. E. Wolf, "Fundamentals of fluorescence and fluorescence microscopy," Methods Cell Biol. **114**, 69–97 (2013).
[155]D. J. Webb and C. M. Brown, "Epi-fluorescence microscopy," Methods Mol. Biol. **931**, 29–59 (2013).
[156]D. Axelrod, Cell-substrate contacts illuminated by total internal reflection fluorescence," J. Cell Biol. **89**, 141–145 (1981).
[157]J. L. Ross, K. Wallace, H. Shuman, Y. E. Goldman, and E. L. Holzbaur, "Processive bidirectional motion of dynein–dynactin complexes *in vitro*," Nat. Cell Biol. **8**, 562–570 (2006).
[158]R. Dixit, J. L. Ross, Y. E. Goldman, and E. L. F. Holzbaur, "Differential regulation of dynein and kinesin motor proteins by tau," Science **319**, 1086–1089 (2008).

[159]H. Shroff, C. G. Galbraith, J. A. Galbraith, H. White, J. Gillette, S. Olenych, M. W. Davidson, and E. Betzig, "Dual-color superresolution imaging of genetically expressed probes within individual adhesion complexes," Proc. Natl. Acad. Sci. U.S.A. **104**, 20308–20313 (2007).
[160]D.-K. Kim, H.-G. Lee, H.-I. Jung, and S.-H. Kang, "Single-protein molecular interactions on polymer-modified glass substrates for nanoarray chip application using dual-color TIRFM," Bull. Korean Chem. Soc. **28**, 783–790 (2007).
[161]K. N. Fish, "Total internal reflection fluorescence (TIRF) microscopy," Curr. Protoc. Cytometry **50**, 12.18.1 (2009).
[162]S. Manley, J. M. Gillette, G. H. Patterson, H. Shroff, H. F. Hess, E. Betzig, and J. Lippincott-Schwartz, "High-density mapping of single-molecule trajectories with photoactivated localization microscopy," Nat. Methods **5**, 155–157 (2008).
[163]E. Hosy, A. Martinière, D. Choquet, C. Maurel, and D.-T. Luu, "Super-resolved and dynamic imaging of membrane proteins in plant cells reveal contrasting kinetic profiles and multiple confinement mechanisms," Mol. Plant **8**, 339–342 (2015).
[164]M. Lei and B. Yao, "Multifunctional darkfield microscopy using an axicon," J. Biomed. Opt. **13**, 044024 (2008).
[165]N. Noda and S. Kamimura, "A new microscope optics for laser dark-field illumination applied to high precision two dimensional measurement of specimen displacement," Rev. Sci. Instrum. **79**, 023704 (2008).
[166]C. Snoeyink and S. Wereley, "Single-image far-field subdiffraction limit imaging with axicon," Opt. Lett. **38**, 625–627 (2013).
[167]A. Curry, W. L. Hwang, and A. Wax, "Epi-illumination through the microscope objective applied to darkfield imaging and microspectroscopy of nanoparticle interaction with cells in culture," Opt. Express **14**, 6535–6542 (2006).
[168]H. Ueno, S. Nishikawa, R. Iino, K. V. Tabata, S. Sakakihara, T. Yanagida, and H. Noji, "Simple dark-field microscopy with nanometer spatial precision and microsecond temporal resolution," Biophys. J. **98**, 2014–2023 (2010).
[169]M. Liu, J. Chao, S. Deng, K. Wang, K. Li, and C. Fan, "Dark-field microscopy in imaging of plasmon resonant nanoparticles," Colloids Surf. B **124**, 111–117 (2014).
[170]L. Xiao, Y. Qiao, Y. He, and E. S. Yeung, "Imaging translational and rotational diffusion of single anisotropic nanoparticles with planar illumination microscopy," J. Am. Chem. Soc. **133**, 10638–10645 (2011).
[171]J. Ortega Arroyo, D. Cole, and P. Kukura, "Interferometric scattering microscopy and its combination with single-molecule fluorescence imaging," Nat. Protoc. **11**, 617–633 (2016).
[172]J. Ortega-Arroyo and P. Kukura, "Interferometric scattering microscopy (iSCAT): New frontiers in ultrafast and ultrasensitive optical microscopy," Phys. Chem. Chem. Phys. **14**, 15625–15636 (2012).
[173]G. Young and P. Kukura, "Interferometric scattering microscopy," Annu. Rev. Phys. Chem. **70**, 301–322 (2019).
[174]R. W. Taylor and V. Sandoghdar, "Interferometric Scattering (iSCAT) Microscopy and Related Techniques," in *Label-Free Super-Resolution Microscopy* (Springer International Publishing, 2019), pp. 25–65.
[175]M. Yu, J. Wang, Y. Yang, C. Zhu, Q. Su, S. Guo, J. Sun, Y. Gan, X. Shi, and H. Gao, "Rotation-facilitated rapid transport of nanorods in mucosal tissues," Nano Lett. **16**, 7176–7182 (2016).
[176]V. P. Chauhan, Z. Popović, O. Chen, J. Cui, D. Fukumura, M. G. Bawendi, and R. K. Jain, "Fluorescent nanorods and nanospheres for real-time *in vivo* probing of nanoparticle shape-dependent tumor penetration," Angew. Chem. Int. Ed. Engl. **50**, 11417–11420 (2011).
[177]K. L. Lee, L. C. Hubbard, S. Hern, I. Yildiz, M. Gratzl, and N. F. Steinmetz, "Shape matters: The diffusion rates of TMV rods and CPMV icosahedrons in a spheroid model of extracellular matrix are distinct," Biomater. Sci. **1**, 581–588 (2013).
[178]S.-J. Li, H.-J. Qian, and Z.-Y. Lu, "Translational and rotational dynamics of an ultra-thin nanorod probe particle in linear polymer melts," Phys. Chem. Chem. Phys. **20**, 20996–21007 (2018).
[179]A. Karatrantos, R. J. Composto, K. I. Winey, and N. Clarke, "Nanorod diffusion in polymer nanocomposites by molecular dynamics simulations," Macromolecules **52**, 2513–2520 (2019).
[180]J. Wang, Y. Yang, M. Yu, G. Hu, Y. Gan, H. Gao, and X. Shi, "Diffusion of rod-like nanoparticles in non-adhesive and adhesive porous polymeric gels," J. Mech. Phys. Solids. **112**, 431–457 (2018).
[181]Y. Han, A. M. Alsayed, M. Nobili, J. Zhang, T. C. Lubensky, and A. G. Yodh, "Brownian motion of an ellipsoid," Science **314**, 626–630 (2006).
[182]K. V. Edmond, M. T. Elsesser, G. L. Hunter, D. J. Pine, and E. R. Weeks, "Decoupling of rotational and translational diffusion in supercooled colloidal fluids," Proc. Natl. Acad. Sci. U.S.A. **109**, 17891–17896 (2012).
[183]G. L. Hunter, K. V. Edmond, M. T. Elsesser, and E. R. Weeks, "Tracking rotational diffusion of colloidal clusters," Opt. Express **19**, 17189–17202 (2011).
[184]D. Mukhija and M. J. Solomon, "Translational and rotational dynamics of colloidal rods by direct visualization with confocal microscopy," J. Colloid Interface Sci. **314**, 98–106 (2007).
[185]T. T. Hormel, S. Q. Kurihara, M. K. Brennan, M. C. Wozniak, and R. Parthasarathy, "Measuring lipid membrane viscosity using rotational and translational probe diffusion," Phys. Rev. Lett. **112**, 188101 (2014).
[186]R. Parthasarathy, "Rapid, accurate particle tracking by calculation of radial symmetry centers," Nat. Methods **9**, 724–726 (2012).
[187]R. M. Dickson, D. J. Norris, and W. E. Moerner, "Simultaneous imaging of individual molecules aligned both parallel and perpendicular to the optic axis," Phys. Rev. Lett. **81**, 5322–5325 (1998).
[188]A. P. Bartko, K. Xu, and R. M. Dickson, "Three-dimensional single molecule rotational diffusion in glassy state polymer films," Phys. Rev. Lett. **89**, 026101 (2002).
[189]J. Jasny and J. Sepioł, "Single molecules observed by immersion mirror objective. A novel method of finding the orientation of a radiating dipole," Chem. Phys. Lett. **273**, 439–443 (1997).
[190]M. Böhmer and J. Enderlein, "Orientation imaging of single molecules by wide-field epifluorescence microscopy," J. Opt. Soc. Am. B **20**, 554–559 (2003).
[191]D. Patra, I. Gregor, and J. Enderlein, "Image analysis of defocused single-molecule images for three-dimensional molecule orientation studies," J. Phys. Chem. A **108**, 6836–6841 (2004).
[192]D. Patra, I. Gregor, J. Enderlein, and M. Sauer, "Defocused imaging of quantum-dot angular distribution of radiation," Appl. Phys. Lett. **87**, 101103 (2005).
[193]J. Enderlein, E. Toprak, and P. R. Selvin, "Polarization effect on position accuracy of fluorophore localization," Opt. Express **14**, 8111–8120 (2006).
[194]Z. Cheng and T. G. Mason, "Rotational diffusion microrheology," Phys. Rev. Lett. **90**, 018304 (2003).
[195]K. Marchuk and N. Fang, "Three-dimensional orientation determination of stationary anisotropic nanoparticles with sub-degree precision under total internal reflection scattering microscopy," Nano Lett. **13**, 5414–5419 (2013).
[196]C. Sönnichsen and A. P. Alivisatos, "Gold nanorods as novel nonbleaching plasmon-based orientation sensors for polarized single-particle microscopy," Nano Lett. **5**, 301–304 (2005).
[197]L. Xiao, Y. Qiao, Y. He, and E. S. Yeung, "Three dimensional orientational imaging of nanoparticles with darkfield microscopy," Anal. Chem. **82**, 5268–5274 (2010).
[198]M. Molaei, E. Atefi, and J. C. Crocker, "Nanoscale rheology and anisotropic diffusion using single gold nanorod probes," Phys. Rev. Lett. **120**, 118002 (2018).
[199]L. He, Y. Li, L. Wei, Z. Ye, H. Liu, and L. Xiao, "Correlation between the translational and rotational diffusion of rod-shaped nanocargo on a lipid membrane revealed by single-particle tracking," Nanoscale **11**, 10080–10087 (2019).
[200]S. Alam and A. Mukhopadhyay, "Translational and rotational diffusions of nanorods within semidilute and entangled polymer solutions," Macromolecules **47**, 6919–6924 (2014).
[201]R. K. Chhetri, R. L. Blackmon, W.-C. Wu, D. B. Hill, B. Button, P. Casbas-Hernandez, M. A. Troester, J. B. Tracy, and A. L. Oldenburg, "Probing biological nanotopology via diffusion of weakly constrained plasmonic nanorods with optical coherence tomography," Proc. Natl. Acad. Sci. U.S.A. **111**, E4289–E4297 (2014).
[202]R. K. Chhetri, K. A. Kozek, A. C. Johnston-Peck, J. B. Tracy, and A. L. Oldenburg, "Imaging three-dimensional rotational diffusion of plasmon

resonant gold nanorods using polarization-sensitive optical coherence tomography," Phys. Rev. E **83**, 040903 (2011).
[203]F. C. Cheong, B. J. Krishnatreya, and D. G. Grier, "Strategies for three-dimensional particle tracking with holographic video microscopy," Opt. Express **18**, 13563–13573 (2010).
[204]J. Sheng, E. Malkiel, and J. Katz, "Digital holographic microscope for measuring three-dimensional particle distributions and motions," Appl. Opt. **45**, 3893–3901 (2006).
[205]J. Fung, K. E. Martin, R. W. Perry, D. M. Kaz, R. McGorty, and V. N. Manoharan, "Measuring translational, rotational, and vibrational dynamics in colloids with digital holographic microscopy," Opt. Express **19**, 8051–8065 (2011).
[206]T. G. Dimiduk, R. W. Perry, J. Fung, and V. N. Manoharan, "Random-subset fitting of digital holograms for fast three-dimensional particle tracking [invited]," Appl. Opt. **53**, G177–G183 (2014).
[207]M. K. Kim, "Principles and techniques of digital holographic microscopy," SPIE Rev. **1**, 018005 (2010).
[208]S.-H. Lee and D. G. Grier, "Holographic microscopy of holographically trapped three-dimensional structures," Opt. Express **15**, 1505–1512 (2007).
[209]J. Garcia-Sucerquia, W. Xu, S. K. Jericho, P. Klages, M. H. Jericho, and H. J. Kreuzer, "Digital in-line holographic microscopy," Appl. Opt. **45**, 836–850 (2006).
[210]S.-H. Lee, Y. Roichman, G.-R. Yi, S.-H. Kim, S.-M. Yang, A. van Blaaderen, P. van Oostrum, and D. G. Grier, "Characterizing and tracking single colloidal particles with video holographic microscopy," Opt. Express **15**, 18275–18282 (2007).
[211]J. L. Nadeau, Y. B. Cho, J. Kühn, and K. Liewer, "Improved tracking and resolution of bacteria in holographic microscopy using dye and fluorescent protein labeling," Front. Chem. **4**, 00017 (2016).
[212]A. Ozcan and E. McLeod, "Lensless imaging and sensing," Annu. Rev. Biomed. Eng. **18**, 77–102 (2016); e-print: https://doi.org/10.1146/annurev-bioeng-092515-010849.
[213]J.-P. Liu, T. Tahara, Y. Hayasaki, and T.-C. Poon, "Incoherent digital holography: A review," Appl. Sci. **8**, 143 (2018).
[214]T. Yanagawa, R. Abe, and Y. Hayasaki, "Three-dimensional mapping of fluorescent nanoparticles using incoherent digital holography," Opt. Lett. **40**, 3312–3315 (2015).
[215]R. Abe and Y. Hayasaki, "Holographic fluorescence mapping using space-division matching method," Opt. Commun. **401**, 35–39 (2017).
[216]F. Verpillat, F. Joud, P. Desbiolles, and M. Gross, "Dark-field digital holographic microscopy for 3D-tracking of gold nanoparticles," Opt. Express **19**, 26044 (2011).
[217]M. Atlan, M. Gross, P. Desbiolles, É. Absil, G. Tessier, and M. Coppey-Moisan, "Heterodyne holographic microscopy of gold particles," Opt. Lett. **33**, 500 (2008).
[218]F. Le Clerc, L. Collot, and M. Gross, "Numerical heterodyne holography with two-dimensional photodetector arrays," Opt. Lett. **25**, 716 (2000).
[219]M. Atlan, M. Gross, and E. Absil, "Accurate phase-shifting digital interferometry," Opt. Lett. **32**, 1456 (2007).
[220]E. Absil, G. Tessier, M. Gross, M. Atlan, N. Warnasooriya, S. Suck, M. Coppey-Moisan, and D. Fournier, "Photothermal heterodyne holography of gold nanoparticles," Opt. Express **18**, 780 (2010).
[221]F. Huang, T. M. P. Hartwich, F. E. Rivera-Molina, Y. Lin, W. C. Duim, J. J. Long, P. D. Uchil, J. R. Myers, M. A. Baird, W. Mothes, M. W. Davidson, D. Toomre, and J. Bewersdorf, "Video-rate nanoscopy enabled by sCMOS camera-specific single-molecule localization algorithms," Nat. Methods **10**, 653–658 (2013).
[222]C. G. Coates, D. J. Denvir, N. G. McHale, K. Thornbury, and M. Hollywood, "Optimizing low-light microscopy with back-illuminated electron multiplying charge-coupled device: Enhanced sensitivity, speed, and resolution," J. Biomed. Opt. **9**, 1244–1252 (2004).
[223]D. Dussault and P. Hoess, "Noise performance comparison of ICCD with CCD and EMCCD cameras," in *Optical Science and Technology, the SPIE 49th Annual Meeting*, edited by E. L. Dereniak, R. E. Sampson, and C. B. Johnson (Denver, CO, 2004), p. 195.
[224]L. Cester, A. Lyons, M. C. Braidotti, and D. Faccio, "Time-of-flight imaging at 10 ps resolution with an ICCD camera," Sensors **19**, 180 (2019).
[225]H. T. Beier and B. L. Ibey, "Experimental comparison of the high-speed imaging performance of an EM-CCD and sCMOS camera in a dynamic live-cell imaging test case," PLoS ONE **9**, e84614 (2014).
[226]L. Rayleigh, "XV. On the theory of optical images, with special reference to the microscope," London, Edinburgh, Dublin Philosophi. Magaz. J. Sci. **42**, 167–195 (1896).
[227]E. Abbe, "Beiträge zur theorie des mikroskops und der mikroskopischen wahrnehmung," Mikroskopische Anatomie **9**, 413–468 (1873).
[228]M. Pellach, J. Goldshtein, O. Ziv-Polat, and S. Margel, "Functionalised, photostable, fluorescent polystyrene nanoparticles of narrow size-distribution," J. Photochem. Photobiol. A Chem. **228**, 60–67 (2012).
[229]J. Fölling, S. Polyakova, V. Belov, A. van Blaaderen, M. L. Bossi, and S. W. Hell, "Synthesis and characterization of photoswitchable fluorescent silica nanoparticles," Small **4**, 134–142 (2008).
[230]H. Ow, D. R. Larson, M. Srivastava, B. A. Baird, W. W. Webb, and U. Wiesner, "Bright and stable core-shell fluorescent silica nanoparticles," Nano Lett. **5**, 113–117 (2005).
[231]I. Tavernaro, C. Cavelius, H. Peuschel, and A. Kraegeloh, "Bright fluorescent silica-nanoparticle probes for high-resolution STED and confocal microscopy," Beilstein J. Nanotechnol. **8**, 1283–1296 (2017).
[232]A. M. Nuruzatulifah, A. A. Nizam, and N. M. N. Ain, "Synthesis and characterization of polystyrene nanoparticles with covalently attached fluorescent dye," Mater. Today: Proc. 5th Int. Conf. Funct. Mater. Devices (ICFMD 2015) **3**, S112–S119 (2016).
[233]J. Kalia and R. T. Raines, "Advances in bioconjugation," Curr. Org. Chem. **14**, 138–147 (2010).
[234]S. Rocha, H. De Keersmaecker, H. Uji-i, J. Hofkens, and H. Mizuno, "Photoswitchable fluorescent proteins for superresolution fluorescence microscopy circumventing the diffraction limit of light," Methods Mol. Biol. **1076**, 793–812 (2014).
[235]M. L. Martin-Fernandez and D. T. Clarke, "Single molecule fluorescence detection and tracking in mammalian cells: The state-of-the-art and future perspectives," Int. J. Mol. Sci. **13**, 14742–14765 (2012).
[236]C. B. Murray, D. J. Norris, and M. G. Bawendi, "Synthesis and characterization of nearly monodisperse CdE (E = sulfur, selenium, tellurium) semiconductor nanocrystallites," J. Am. Chem. Soc. **115**, 8706–8715 (1993).
[237]W. K. Bae, K. Char, H. Hur, and S. Lee, "Single-step synthesis of quantum dots with chemical composition gradients," Chem. Mater. **20**, 531–539 (2008).
[238]A. M. Munro, J. A. Bardecker, M. S. Liu, Y.-J. Cheng, Y.-H. Niu, I. J.-L. Plante, A. K.-Y. Jen, and D. S. Ginger, "Colloidal CdSe quantum dot electroluminescence: Ligands and light-emitting diodes," Microchim. Acta **160**, 345–350 (2008).
[239]A. L. Efros and D. J. Nesbitt, "Origin and control of blinking in quantum dots," Nat. Nanotechnol. **11**, 661–671 (2016).
[240]W. Haiss, N. T. K. Thanh, J. Aveyard, and D. G. Fernig, "Determination of size and concentration of gold nanoparticles from UV-vis spectra," Anal. Chem. **79**, 4215–4221 (2007).
[241]Y.-H. Lin, W.-L. Chang, and C.-L. Hsieh, "Shot-noise limited localization of single 20 nm gold particles with nanometer spatial precision within microseconds," Opt. Express **22**, 9159–9170 (2014).
[242]T. Sannomiya and J. Vörös, "Single plasmonic nanoparticles for biosensing," Trends Biotechnol. **29**, 343–351 (2011).
[243]A. Jayaraman, "Polymer grafted nanoparticles: Effect of chemical and physical heterogeneity in polymer grafts on particle assembly and dispersion," J. Polym. Sci. Part B Polym. Phys. **51**, 524–534 (2013).
[244]I. A. Rahman and V. Padavettan, "Synthesis of silica nanoparticles by sol-gel: Size-dependent properties, surface modification, and applications in silica-polymer nanocomposites—A review," J. Nanomater. **2012**, 1–15 (2012).
[245]J. R. Nicol, D. Dixon, and J. A. Coulter, "Gold nanoparticle surface functionalization: A necessary requirement in the development of novel nanotherapeutics," Nanomedicine **10**, 1315–1326 (2015).

[246]E. Imbert-Laurenceau, M.-C. Berger, G. Pavon-Djavid, A. Jouan, and V. Migonney, "Surface modification of polystyrene particles for specific antibody adsorption," Polym. Collect. Papers from PDM 2004. Polym. Dispersed Media - Colloids: Preparation Appl. **46**, 1277–1285 (2005).
[247]D. R. Breed, R. Thibault, F. Xie, Q. Wang, C. J. Hawker, and D. J. Pine, "Functionalization of polymer microspheres using click chemistry," Langmuir **25**, 4370–4376 (2009).
[248]W. Liu, M. Howarth, A. B. Greytak, Y. Zheng, D. G. Nocera, A. Y. Ting, and M. G. Bawendi, "Compact biocompatible quantum dots functionalized for cellular imaging," J. Am. Chem. Soc. **130**, 1274–1284 (2008).
[249]A. S. Ethiraj, N. Hebalkar, S. K. Kulkarni, R. Pasricha, J. Urban, C. Dem, M. Schmitt, W. Kiefer, L. Weinhardt, S. Joshi, R. Fink, C. Heske, C. Kumpf, and E. Umbach, "Enhancement of photoluminescence in manganese-doped ZnS nanoparticles due to a silica shell," J. Chem. Phys. **118**, 8945–8953 (2003).
[250]J. Qian, Y. Wang, X. Gao, Q. Zhan, Z. Xu, and S. He, "Carboxyl-functionalized and bio-conjugated silica-coated quantum dots as targeting probes for cell imaging," J. Nanosci. Nanotechnol. **10**, 1668–1675 (2010).
[251]A. H. Fischer, K. A. Jacobson, J. Rose, and R. Zeller, "Preparation of slides and coverslips for microscopy," Cold. Spring Harb. Protoc. **2008**, pdb.prot4988 (2008).
[252]J. W. Swan and J. F. Brady, "Particle motion between parallel walls: Hydrodynamics and simulation," Phys. Fluids **22**, 103301 (2010).
[253]T. Savin and P. S. Doyle, "Static and dynamic errors in particle tracking microrheology," Biophys. J. **88**, 623–638 (2005).
[254]A. E. Burgess, The rose model, revisited," J. Opt. Soc. Am. A, Opt., Image Sci., Vision **16**, 633–646 (1999).
[255]J. C. Waters, "Accuracy and precision in quantitative fluorescence microscopy," J. Cell. Biol. **185**, 1135–1148 (2009).
[256]U. Kubitscheck, "Fluorescence Microscopy: Single Particle Tracking," in *Encyclopedic Reference of Genomics and Proteomics in Molecular Medicine* (Springer, Berlin, 2006), pp. 579–583.
[257]R. H. Webb, "Confocal optical microscopy," Rep. Progre. Phys. **59**, 427 (1996).
[258]J. C. Crocker and E. R. Weeks, "Particle tracking using IDL," see http://www.physics.emory.edu/faculty/weeks//idl/tracking.html.
[259]D. Blair and E. Dufresne, "The matlab particle tracking code repository," (2008).
[260]D. Allan, C. van der Wel, N. Keim, T. A. Caswell, D. Wieker, R. Verweij, C. Reid, Thierry, L. Grueter, K. Ramos, apiszcz zoeith, R. W. Perry, F. Boulogne, P. Sinha, pfigliozzi, N. Bruot, L. Uieda, J. Katins, H. Mary, and A. Ahmadia, "Soft-matter/trackpy: Trackpy v0.4.2," Zenodo (2019).
[261]M. Molaei and J. Sheng, "Imaging bacterial 3D motion using digital in-line holographic microscopy and correlation-based de-noising algorithm," Opt. Express **22**, 32119–32137 (2014).
[262]N. Chenouard, I. Smal, F. de Chaumont, M. Maška, I. F. Sbalzarini, Y. Gong, J. Cardinale, C. Carthel, S. Coraluppi, M. Winter, A. R. Cohen, W. J. Godinez, K. Rohr, Y. Kalaidzidis, L. Liang, J. Duncan, H. Shen, Y. Xu, K. E. G. Magnusson, J. Jaldén, H. M. Blau, P. Paul-Gilloteaux, P. Roudot, C. Kervrann, F. Waharte, J.-Y. Tinevez, S. L. Shorte, J. Willemse, K. Celler, G. P. van Wezel, H.-W. Dan, Y.-S. Tsai, C. O. de Solórzano, J.-C. Olivo-Marin, and E. Meijering, "Objective comparison of particle tracking methods," Nat. Methods **11**, 281–289 (2014).
[263]M. K. Cheezum, W. F. Walker, and W. H. Guilford, "Quantitative comparison of algorithms for tracking single fluorescent particles," Biophys. J. **81**, 2378–2388 (2001).
[264]F. Ruhnow, D. Zwicker, and S. Diez, "Tracking single particles and elongated filaments with nanometer precision," Biophys. J. **100**, 2820–2828 (2011).
[265]K. A. Lidke, B. Rieger, T. M. Jovin, and R. Heintzmann, "Superresolution by localization of quantum dots using blinking statistics," Opt. Express **13**, 7052 (2005).
[266]H. Yücel and N. T. Okumuşoğlu, "A new tracking algorithm for multiple colloidal particles close to contact," J. Phys.: Condens. Matter **29**, 465101 (2017).
[267]N. Chenouard, I. Bloch, and J.-C. Olivo-Marin, "Multiple hypothesis tracking in cluttered condition," in *2009 16th IEEE International Conference on Image Processing (ICIP)* (IEEE, Cairo, 2009), pp. 3621–3624.
[268]N. Chenouard, I. Bloch, and J.-C. Olivo-Marin, "Multiple hypothesis tracking in microscopy images," in *2009 IEEE International Symposium on Biomedical Imaging: From Nano to Macro* (IEEE, Boston, MA, 2009), pp. 1346–1349.
[269]J. W. R. Mellnik, M. Lysy, P. A. Vasquez, N. S. Pillai, D. B. Hill, J. Cribb, S. A. McKinley, and M. G. Forest, "Maximum likelihood estimation for single particle, passive microrheology data with drift," J. Rheol. (N. Y. N. Y) **60**, 379–392 (2016).
[270]E. J. Fong, Y. Sharma, B. Fallica, D. B. Tierney, S. M. Fortune, and M. H. Zaman, "Decoupling directed and passive motion in dynamic systems: Particle tracking microrheology of sputum," Ann. Biomed. Eng. **41**, 837–846 (2013).
[271]L. Van Hove, "Correlations in space and time and born approximation scattering in systems of interacting particles," Phys. Rev. **95**, 249–262 (1954).
[272]P. Hopkins, A. Fortini, A. J. Archer, and M. Schmidt, "The van Hove distribution function for Brownian hard spheres: Dynamical test particle theory and computer simulations for bulk dynamics," J. Chem. Phys. **133**, 224505 (2010).
[273]Y. Virkar and A. Clauset, "Power-law distributions in binned empirical data," Ann. Appl. Stat. **8**, 89–119 (2014).
[274]A. Rahman, "Correlations in the motion of atoms in liquid argon," Phys. Rev. **136**, A405–A411 (1964).
[275]W. K. Kegel and a. A. van Blaaderen, "Direct observation of dynamical heterogeneities in colloidal hard-sphere suspensions," Science **287**, 290–293 (2000).
[276]A. Aufderhorst-Roberts, W. J. Frith, and A. M. Donald, "A microrheological study of hydrogel kinetics and micro-heterogeneity," Eur. Phys. J. E **37**, 44 (2014).
[277]H. A. Houghton, I. A. Hasnain, and A. M. Donald, "Particle tracking to reveal gelation of hectorite dispersions," Eur. Phys. J. E **25**, 119–127 (2008).
[278]T. Savin and P. S. Doyle, "Statistical and sampling issues when using multiple particle tracking," Phys. Rev. E. **76**, 021501 (2007).
[279]J. P. Rich, G. H. McKinley, and P. S. Doyle, "Size dependence of microprobe dynamics during gelation of a discotic colloidal clay," J. Rheol. **55**, 273–299 (2011).
[280]M. T. Valentine, P. D. Kaplan, D. Thota, J. C. Crocker, T. Gisler, R. K. Prud', M. Beck, and D. A. Weitz, "Investigating the microenvironments of inhomogeneous soft materials with multiple particle tracking," Phys. Rev. E. **64**, 061506 (2001).
[281]J. M. Newby, A. M. Schaefer, P. T. Lee, M. G. Forest, and S. K. Lai, "Convolutional neural networks automate detection for tracking of submicron-scale particles in 2D and 3D," Proc. Natl. Acad. Sci. U.S.A. **115**, 9026–9031 (2018).
[282]E. Moen, D. Bannon, T. Kudo, W. Graf, M. Covert, and D. Van Valen, "Deep learning for cellular image analysis," Nat. Methods. **16**, 1233–1246 (2019).
[283]W. Ouyang, A. Aristov, M. Lelek, X. Hao, and C. Zimmer, "Deep learning massively accelerates super-resolution localization microscopy," Nat. Biotechnol. **36**, 460–468 (2018).
[284]S. Helgadottir, A. Argun, and G. Volpe, "Digital video microscopy enhanced by deep learning," Optica **6**, 506–513 (2019).
[285]Y. Yao, I. Smal, and E. Meijering, "Deep neural networks for data association in particle tracking," in *2018 IEEE 15th International Symposium on Biomedical Imaging (ISBI 2018)* (IEEE, Washington, DC, 2018), pp. 458–461.
[286]N. Granik, L. E. Weiss, E. Nehme, M. Levin, M. Chein, E. Perlson, Y. Roichman, and Y. Shechtman, "Single-particle diffusion characterization by deep learning," Biophys. J. **117**, 185–192 (2019).
[287]P. Kowalek, H. Loch-Olszewska, and J. Szwabiński, "Classification of diffusion modes in single-particle tracking data: Feature-based versus deep-learning approach," Phys. Rev. E. **100**, 032410 (2019).
[288]Y. Matsuda, I. Hanasaki, R. Iwao, H. Yamaguchi, and T. Niimi, "Estimation of diffusive states from single-particle trajectory in heterogeneous medium using machine-learning methods," Phys. Chem. Chem. Phys. **20**, 24099–24108 (2018).